Fall 2011

Control of a large scale wind turbine utilizing a fluid drive

Matthew Foley
University of New Hampshire, Durham

CONTROL OF A LARGE SCALE WIND TURBINE UTILIZING A FLUID DRIVE

MATTHEW FOLEY

B.S. Electrical Engineering, Florida Institute of Technology, 1998

THESIS

Submitted to the University of New Hampshire

in Partial Fulfillment of

the Requirements for the Degree of

Master of Science

in

Electrical Engineering

September, 2011

ProQuest LLC
789 East Eisenhower Parkway
P.O. Box 1346
Ann Arbor, MI 48106-1346

ACKNOWLEDGEMENTS

I am dedicating this thesis and research to my two grandchildren Gregory Dean and Lexey Grace. It is my hope that through this research I can help to leave them with a better world than the one that we inherited. I also want to specifically thank my wife Diane who has supported me through this three year long endeavor. She has had to put up with countless late nights and to some extent my absence from family functions that allowed me the time needed to fulfill my Masters degree requirements. It is a special testament to her that we have been able to endure my working 45^{+} hour weeks, going to class, and the far too numerous family crises that have not only interrupted our lives, but also at times have become the norm of our lives over these past three years.

Finally, I would like to thank Dr. L.G. Kraft for giving me the motivation and the direction to see this thesis through to completion. He was able to recognize the high stress levels that I was under at times and provide the timely pep talks that I needed to stay motivated.

A special thanks to the financial and educational sponsors of this research:

HiRel Systems, LLC

UNH Electrical and Computer Engineering Department

FOREWORD

It is not often in an engineering career that you are given the opportunity to look at a problem and are given a blank slate from which to develop an optimal solution. More often than not the role of an engineer is to put out the immediate fires and bring the production lines or system back up to working order. The solutions that are developed are often the most expedient and cost effective that can be derived. It is challenging to change the gears in your mind to go from crisis solution management to a research and development study, to step back from the problem and analyze it slightly differently.

Wind power has been around since ancient times, and the reality is that even with our modern technology we have changed the basic design very little over the past 700 – 800 years. That leads to the current state of wind turbine development in which everyone is rushing to try and solve the problem of gearbox failure. Most engineers operate in a crisis solution role. The solutions that they develop are centered on what they can do quickly and easily. For this reason there are a number of papers on advanced control techniques and studies of gearbox fabrication materials. This thesis, while not completely coming from a blank slate, allows the entire system to be reviewed and where appropriate suggest radical changes that cannot be analyzed in the normal production environment.

This thesis borrows technologies from other industries and incorporates them into current wind turbine models. Specifically, the idea for this thesis is to use the developments made in the marine and land transportation industries in hydraulic couplers and incorporate them into the drive train of a wind turbine. The fluid drive technology has been proven at the multi-megawatt level. The fluid drive inherently absorbs vibration energy at frequencies that are harmful to gearboxes.

This brings about the question, "Why has this not been looked at previously?" The reason for this is simple: humans do not like change. As proof of this all we need to do is look to our current automobiles. The technology for automatic transmissions existed over 100 years ago, but it was not until the 1940's that a major car manufacturer put them into their production models. Furthermore it was another 40 years until the automatic transmission gained the full acceptance of the population. The old adage of "If it isn't broken, don't fix it" applies to not only to the evolution of our cars but also to the wind turbine drive train.

The wind turbine problem has rarely been viewed as a drive train issue, but normally as a gearbox issue. For that reason, implementing changes in the drive train itself to minimize torque variations is met with the standard human emotion of resistance. Hopefully the research presented here will help to reduce some of that resistance, and bring us to the ultimate goal of solving the gearbox failure problem, and to an economically feasible model to allow wind energy to prosper and contribute in an ever changing energy cost model.

TABLE OF CONTENTS

LIST OF FIGURES

LIST OF TABLES

NOMENCLATURE

NREL – National Renewable Energy Laboratory

FAST – Fatigue Aerodynamic Structures and Turbulence software

VAWT – Vertical Axis Wind Turbine

HAWT – Horizontal Axis Wind Turbine

HSS – High Speed Shaft

LSS – Low Speed Shaft

PI – Proportional-Integral (control)

K_p - Proportional Gain

K_t - Integral Gain

LQR – Linear Quadratic Regulator

Q – State Penalty Matrix

R – Input Penalty Matrix

J – Cost Function

Λ - System Eigenvalues

$\underline{x}$ – State Vector

$\underline{u}$ – Input Vector

$\underline{A}$ – State Matrix

$\underline{B}$ – Input Matrix

$\underline{K}$ – Gain Matrix

RMS – Root Mean Square

STD – Standard Deviation

VARIABLES AND UNITS

Variable Name	Symbol	Alternate	Units
Mass (all 3 blades)	M_b		kg
Inertia (all 3 blades)	J_b		kg-m^2
Blade Drag Constant	B_b		Nm/(rad/sec)
Blade Damping Coefficient	D_b		Nm/(rad/sec)
Blade Spring Constant	K_b		Nm/rad
Inertia of the Rotor	J_r		kg-m^2
Rotor Friction Loss	B_r		Nm/(rad/sec)
Rotor Torsion Damping	D_r		Nm/(rad/sec)
Rotor Spring Constant	K_r		Nm/rad
Fluid Inertia	J_f		kg-m^2
Laminar Fluid Losses	B_f		Nm/(rad/sec)
Fluid Damping Coefficient	D_f		Nm/(rad/sec)
Fluid Spring Constant	K_f		Nm/rad
Generator Inertia	J_g		kg-m^2
Equivalent Friction Drag on Generator	B_f		Nm/(rad/sec)
Rated Output Power	P_o		Watts
Blade Actuator Time Constant	τ_b	tauB	Secs
Fluid Coupler Time Constant	τ_f	tauF	mSecs
Gear Ratio	N		-
Low Speed Shaft Velocity	$\dot{\theta}_{LSS}$		rad/sec
High Speed Shaft Velocity	$\dot{\theta}_{HSS}$		rad/sec
Low Speed Shaft Torque	T_{LSS}		Nm

Blade Tip Rotational Acceleration	$\ddot{\theta}_1$		$\mathrm{rad/sec^2}$
Blade Tip Rotational Velocity	$\dot{\theta}_1$		rad/sec
Blade Tip Rotational Position	θ_1		rad
Rotor Rotational Acceleration	$\ddot{\theta}_2$		$\mathrm{rad/sec^2}$
Rotor Rotational Velocity	$\dot{\theta}_2$		rad/sec
Rotor Rotational Position	θ_2		rad
Fluid Coupler Acceleration	$\ddot{\theta}_3$		$\mathrm{rad/sec^2}$
Fluid Coupler Velocity	$\dot{\theta}_3$		rad/sec
Fluid Coupler Position	θ_3		rad
Gearbox Jerk	$\dddot{\theta}_4$		$\mathrm{rad/sec^3}$
Gearbox Rotational Acceleration	$\ddot{\theta}_4$		$\mathrm{rad/sec^2}$
Gearbox Rotational Velocity	$\dot{\theta}_4$		rad/sec
Gearbox Rotational Position	θ_4		Rad
Generator Rotational Acceleration	$\ddot{\theta}_{4g}$		$\mathrm{rad/sec^2}$
Generator Rotational Velocity	$\dot{\theta}_{4g}$		rad/sec
Wind Speed	W_s		m/sec
Torque From the Wind Speed	T_w		Nm
Torque Applied to the Generator	T_g		Nm
Blade Pitch Angle Command Signal	B		Deg
Solenoid Valve Position Command	F		Inches

ABSTRACT

CONTROL A OF LARGE SCALE WIND TURBINE UTILIZING A FLUID DRIVE

by:

Matthew Foley

University of New Hampshire, September, 2011

As wind turbines grow in size there are added strains within the mechanical structure that need to be mitigated to improve machine life. The current area of greatest concern is the premature failure of the gearbox box due to torque variations along the drive train. This thesis incorporates a fluid coupler into the turbine's drive train. Three different controllers are developed for this model with the goal of minimizing the torque variations seen by the gearbox and providing better generator speed regulation.

The result of this study shows that the addition of the fluid coupler is a major improvement to the system. The coupler removes a resonant peak from the transfer function and allows for better speed regulation. Because of this a standard PI-Controller provides good system level performance. The performance can be improved with state feedback controllers, but these are not a necessity when a fluid coupler is present.

CHAPTER 1

A BRIEF HISTORY OF WIND POWER FROM EARLY TO MODERN TIMES AND FUTURE CHALLENGES

History of Early Wind Power

Humans have been using wind power throughout recorded history. The earliest use of wind mills appeared in Persia. These wind mills were Vertical Axis Wind Turbines (VAWT) with the blades constructed of sheets of cloth or reeds (1). The wind mills were largely used for grinding grain and pumping water from wells to allow for crop irrigation. The VAWT of the past suffer from the same problems that VAWTs do today. Because of their configuration, the wind power is concentrated on the upwind blade(s), and the downwind blade(s) (or sail) remains in the wind shadow. This causes a tremendous amount of mechanical stress on the system and is one of the major reasons for system failure both in ancient times and today.

In the early 1300's AD there was a major change in the construction philosophy of wind turbines. In Western Europe the postmill style windmill was created. This design incorporates the use of a horizontal sail and a gearbox to translate the horizontal motion to a vertical motion. The design of these windmills was largely based on the design of the horizontally mounted waterwheels used throughout Europe. The Dutch

further enhanced this design by placing these horizontal windmills on towers with rotating tops. This represented a significant advancement in wind power technology (2). The rotating design allowed the blades of the windmill to be pointed directly into the wind and greatly improved the efficiency of the machines. Because the machines were allowed to rotate into an upwind direction there was the elimination of the wind shadow of building or sails as with the earlier designs of the postmill or VAWT.

The new Dutch style wind mills were not without their drawbacks. The older VAWT and postmill style windmills were fixed position structures, and could not be optimized for power generation (in this case mechanical power). The new Dutch designs required the blades to be physically moved into an upwind position. This means that the machines could not be run passively. The requirement for the tower axis yaw to be controlled, lead to the development of living quarters within the windmills themselves so that an operator could actively turn the blades into or out of the wind as conditions dictated. This is a design parameter that has carried forward to modern HAWT, although the mechanism for actively controlling the yaw of the machine is now done with active servomotors and electronic feedback controllers. The active upwind control of modern wind turbines allows the machine to not only optimize the power generated from the wind, but also eliminates the wind shadowing of the tower. It is the wind shadowing that caused the majority of complaints about modern wind turbines as the blades would "unload" when they passed behind the tower and resulted in unpleasant sonic vibrations.

The technological advantages gained by the yaw controlled windmills led to advances in the blade design. Blade design progressed from the early fixed sail designs to designs that incorporated the majority of modern elements that are considered critical in modern blade design. Eventually the blades used on the windmills incorporated elements of early airfoil design. This included such items as creating a leading and trailing edge, repositioning the center of gravity of the blade, and giving the blades nonlinear twists.

Modern Developments of Wind Power Electricity Generation

The switch from using the wind to do mechanical work to using the wind to create electricity is marked by the development of Charles F. Brush's wind power generator in 1888 (3). This machine was a fixed axis (postmill style) machine which featured a blade diameter of 17 feet and a 50:1 gearbox used to drive a DC generator. The major drawback of this original electricity generating turbine was that the rotor speeds were too low to offer an economically practical electricity generating solution.

This initial problem was solved in 1891 by a Danish physicist Poul La Cour. He coupled the design elements of the Dutch windmills along with the principles of aerodynamic lift and drag to create a windmill capable of spinning at substantially faster speeds. Because he was able to get faster turbine speeds, he was able to create output powers in the neighborhood of 25 kW. This allowed enough power to be generated such that it was practical to provide electricity to small towns throughout Denmark. His design gained enough widespread acceptance that by the end of World War I there were approximately 250 electricity producing wind generators throughout Denmark (3).

The wind generator industry in the United States followed a different path than that of the Danes. Throughout the early 1900's much of the rural US was not connected to the power grid. As a way of supplying power to these areas a large number of smaller 1-3 kW turbines were manufactured. The blades of these smaller turbines were inspired by aircraft propellers and spun at high rates of speed (3). Because of the light population densities of the Midwest, these machines gained widespread usage at farms and homesteads. These small generators allowed the farmers in these areas to charge batteries and power small radios. The popularity of these smaller generators continued through the 1920's and 30's, but the desire to have more available power and the Great Depression led to their demise. One of the federal government's stimulus packages was to provide for the electrification of rural areas throughout the US. With many homes now connected directly to the grid, the need for these smaller wind turbines essentially disappeared.

With the change away from the smaller point of use wind turbines, a much more ambitious project was undertaken. In 1934, an engineer from Cape Cod, Palmer Putnan, developed a concept for a wind turbine of a much larger scale. With funding from the S. Morgan Smith Company of York, PA, he was able to develop a wind turbine rated at 1.25 MW. The turbine was constructed on a hill called Grandpa's Knob near Rutland, VT in 1941, and operated for four years before one of the blades broke off near the hub (3). While this project was a success, it did highlight the engineering limitations of the materials that were available for construction of these types of devices at the time.

Unfortunately, the success of the wind generator at Grandpa's Knob was not duplicated for almost another 30 years. Following the end of World War II, gas and oil prices returned to levels that made wind power electricity generation unsustainable from an economic standpoint. For that reason much of the research that was dedicated to making more efficient machines ceased and instead the focus was on steam power generation. It was not until "The 6-Day War" between Egypt and Israel in 1973 that wind power again gained national attention.

As a result of the war, the oil rich countries of the Middle East, acting as OPEC, instituted an oil embargo on all of the countries supporting Israel. The resulting gas and oil shortages throughout Europe and the United States brought attention to the fact that they were too dependent upon fuel from foreign nations. The result was that there was a renewed effort and focus to develop power sources that were not dependent on oil. During this time a considerable amount of time and resources were dedicated to developing commercially viable alternatives to oil based power generation.

Unfortunately much of this dedication to alternative forms of energy was short-lived. The oil policies under the Reagan administration and oil production efficiency improvements brought oil prices back to economically sustainable levels. These levels held until the oil run up in 2008. These lower fuel prices led the US to largely abandon much of its research into alternative forms of energy, while the European countries continued wind technology research, albeit at a much slower pace. Because the European nations continued their research into wind technology, most of the wind generator companies and advancements have come from their efforts. The US wind

energy industry did not see large scale development until policy changes at the state and federal level began to demand that a greater percentage of supplied power come from renewable resources including wind power, and these policies provided tax incentives for companies to install renewable energy sources. It is likely that without this long term policy change the normal economic pressures would keep wind energy installations at or near the plateaus reached in the 1990's and there would have been crisis reaction to the oil price spike in 2008 that would have resulted in yet another short term focus on renewable energy until prices stabilized.

Current Status of Wind Power Generation

There have been a number of milestones met in the United States as we continue to add wind generator capacity to our electric grid. As of the end of June 2010, the United States had added a total of 1.2 GW of wind energy capacity, thus bringing its current wind generation total to slightly more than 36.3 GW. (4). Despite the steady growth seen in the US we are very quickly falling behind the pace of China and the European Union (EU) in terms of installing new capacity. During this same time period China installed 7.8 GW of additional capacity to bring their total capacity to 33.8 GW and the EU installed and additional 2.9 GW. While the US remains the world leader in wind generated energy, it will soon be passed as other countries continue to install generation capacity at much higher rates.

Despite the increases seen in other places around the world there have still been significant milestones reached in the US market. The state of Iowa has now reached the goal of generating over 20% of its electricity from wind energy, and the Cape Wind

Offshore wind project has been given the final approvals to install the first offshore wind farm in the US.

Given all these developments, there continues to be a number of obstacles impeding the process of getting to the desired installation rate of 16 GW per year starting in 2018. One of the biggest obstacles now facing the industry is management of the supply chain. Currently nearly 50% of the component vendors are on-shore in the US. However, a number of new facilities need to be brought on-line to fulfill the ever increasing need for steel and the turbine blades. In efforts to fill some of these voids, a new foundry is being built in Kansas, and ground work has been laid for a new blade manufacturing facility in Massachusetts. Despite these improvements to the supply chain, the US industry remains dependent on the offshore market for many of the electrical components of the turbines. As other regions around the world continue to increase their installed capacity, these components will become the next bottleneck in the supply chain and will require action that should bring additional manufacturing back to the US.

The other area of wind power generation that continues to plague the industry is that of gearbox failure. The initial design goal of the industry was to create a gearbox that would operate reliably for 20 years. Unfortunately, this is not the reality of the current state. On average gearboxes need to be replaced every 5-7 years, and account for approximately 15 – 20% of the total operating costs of the wind turbine (5). This cost represents not only a typical amortization of the gearbox replacement but also the standard maintenance required by the gearbox including lubrication, seal replacement,

pump maintenance and clutches. Another major factor is that the gearbox itself is one of the higher cost components in the system. A typical gearbox and electronic assembly account for nearly 25% of the initial capital investment in a wind turbine (4). Because this problem is so well documented throughout the industry, numerous studies have been undertaken in both the public and private sectors to try and eliminate the gearbox failures. One of the newest projects undertaken is a $45 million grant given to Clemson University under the Economic Stimulus package of 2009 (6). This grant will allow for the construction of a facility that will be able to test the next generation of wind turbine gearboxes. This facility's goal is to be able to fatigue test gearboxes in the 7 – 15 MW range.

Wind Energy Challenges and the Future

In the coming years the next large hurdles that the wind industry must tackle are related to developing large scale wind turbines in offshore locations. Offshore wind turbines hold many economic advantages (once completed) over their onshore counter parts, and they are one of the major contributors in the plan for 20% of electrical power from wind in 2030 (7). One of the advantages is that offshore wind can be located much closer to population centers than onshore wind farms. This has to do with the wind power available in locations just off the coast. The ocean and large water bodies have a distinct advantage over land locations in that there are no obstacles impeding the speed of the wind. Therefore shorter towers can be used to generate the same amount of power. Because of this lower wind resistance, higher wind speeds are maintained across a more consistent area. The power available from the wind is related to the wind

speed cubed and the rotator diameter squared. (8) However the wind needs to be steady and omni-directional for reliable power generation.

At present, land-based wind farms far outnumber the offshore farms, and are also considerably larger. Currently, the only offshore wind farms to be constructed are in Europe, mainly located in The United Kingdom and on the North and Baltic Seas near Scandinavia. The majority of the European offshore wind farms are of the shallow water variety. This means that they are on fixed platforms, in water that is less than 30m deep. Currently there is a single turbine platform for deep water power generation under construction.

One of the reasons for the slow development of these offshore wind farms is that the infrastructure is not in place to allow for their development. Special barges and floating cranes are needed to lift the nacelle and rotors to the tops of these offshore towers. Another of the challenges facing offshore wind power is the lack of a defined platform that would allow the wind farms to be moved further out into the ocean, similar to deep sea oil wells. The current design of these platforms is for shallow water power generation and they consist of concrete pilings set upon the sea floor, and currently are limited to around 30m. Future wind turbines located outside of the continental shelf or in deeper water will require the development of a standard platform that is either a ballast or barge design. Either of these new designs will be subject to additional control requirements so that they can remain connected to the high voltage grid, meaning that they will have to be held in place. One of the suggested methods for maintaining this position control is to duplicate the controls used on deep

water oil platforms that use microburst controllers and GPS to keep the unit centered over the desired location.

Another of the major challenges that wind power generation faces is that the generators are starting to reach their practical size limit for land based applications. Currently this limit is around 10 MW, with a blade sweep diameter of 475 feet. The issue with going to larger turbines for onshore applications is that materials required to build the larger generators cannot be transported to the construction site from the originating factory. The blades and tower components need to be able to travel either by rail or truck to their final destination and are therefore limited by train tunnels and highway overpass sizes. In each case the maximum height of any component is limited to approximately 4.2m (7). This creates the issue of potentially building components on site, which would be an extremely costly proposition, or creating sectioned blades or tower components which present numerous other structural design challenges. Because of these constraints, the next leaps in wind turbine size are more likely to be seen in offshore wind applications where transportation to the construction sites can be done by barge, and the transportation restrictions largely disappear.

The final hurdle in the economic viability of large scale wind power generation is the capacity factor of the wind turbines themselves. The current average capacity factor of wind turbines is around 25%. That means a turbine rated for 1 MW is on average producing only about 250 kW. There are a number of different factors in these low capacity figures. Some are related to weather/wind speed and are outside of human control. The other major contributor to the low average capacity factor is the down

time of machines due to maintenance, and most of the maintenance activity is focused around the gearboxes. The gearboxes are the weak link in the windmill drive train as they have to transfer the slowly rotating, large torques generated in the blade and rotor to a high speed, low torque generator. The gears transfer power through relatively small teeth that are subject to breaking and micro-pitting of the metal. This leads to gearbox failures that are in the 5-7 year range instead of the 20 years that they are intended to operate (7).

The gearbox failures that are noted above are not limited to just the wind industry. Similar issues are present in the marine transportation industry, where large, faster spinning power plants need to drive slower spinning high torque propellers. In this industry, torque variations making their way through to the propeller causes cavitation, which makes the ship very noisy, and does not allow power to be applied to moving the ship forward. In order to get around this problem, the industry implemented a fluid coupling between the power plant and the propeller. The fluid coupling allows for an extra degree of control of the system. The fluid acts like a damper by absorbing some of the torque variations in the drive train.

The rest of the focus of this paper will be on implementing a similar fluid coupler into the drive train of a wind powered generator. By limiting the torque variations on the gearbox through the fluid coupling, the gearbox lifetime can be improved. Furthermore, the fluid coupler has the added dynamic of allowing for an additional input control on the system. This is maintained through the positioning of the solenoid valve within the coupler itself. The added control allows for the implementation of

more advanced controllers such as pole-placement or liner quadratic regulators (LQR) to limit the torque variations along the drive train more than the industry standard Proportional-Integral (PI) controller is capable of doing.

CHAPTER 2:

MODEL AND PI CONTROL DEVELOPMENT

Modeling Overview and Generation of Control Algorithm

This Chapter will develop a linearized model for a 5 MW wind turbine. The equations of motion are converted to state-space representation. The newly derived linear model includes the components of a fluid coupling drive. The fluid coupling transmits a constant torque to the generator and gearbox side of the wind turbine. This model has not yet been formally characterized for systems of this size, and therefore there is not a base-line model to compare the advanced forms of controllers against. In an effort to provide a base-line performance of the system, a Proportional-Integral (PI) controller will be developed. The PI controller is the current standard control technique used in wind turbines due to its ability to control the system based only on the output speed of the generator. By careful selection of the proportional and integral gains, a stable system can be maintained with minimal need for measuring the states of all of the other elements within the system. The advanced controllers discussed later, pole-placement and the linear quadratic regulator, require the outputs from all of the states developed from the equations of motion. The inclusion of the additional states allows the advanced controllers to better mitigate torque variations propagating themselves along the drive train.

Development of a System Model

There have been many linear and non-linear models of large and small wind turbines in an effort to understand the different dynamics of the system. The model used in this thesis originated at NREL. In a previous thesis at UNH, Jacob Aho reduced the non-linear full scale model to a linear model. (9) Jacob's model has been extended to include a fluid coupler. A linear model of the wind turbine is shown below in Figure 2.1.

The model developed for this wind turbine is simplified in the sense that many of the non-linear elements of the dynamic system have either been ignored or lumped into one of the rotational elements within the model. This simplified model, without the fluid coupler, has been previously compared with the Fatigue Aerodynamics Structures and Turbulence (FAST) model developed by the National Renewable Energy Laboratory (NREL) in Colorado. A review of the thesis written by Jacob Aho in May of 2010 shows a comparison of the base model with that of the FAST model and provides a detailed analysis that concludes that the simplified model used for this thesis is an adequate approximation of the real wind turbine system. All of the elements within this system are assumed to be rotational masses, dampers or torsion springs.

The new model presented in this thesis builds upon the data gathered by Jacob Aho and NREL. The rotational elements and values for the blades, rotor, gearbox and generator are copied from the earlier work. In this thesis a fluid coupler is inserted between the low speed shaft and the gearbox. The fluid coupler is assumed to be largely damping, with a small spring force in parallel. By nature of the fluid coupler, any

torque variations that are propagated to the low speed shaft will be dissipated in the fluid coupler. This dissipation will take on the form of heat, which must be externally removed via cooling apparatus within the fluid coupler structure.

Figure 2.1 – Simplified Wind Turbine Model

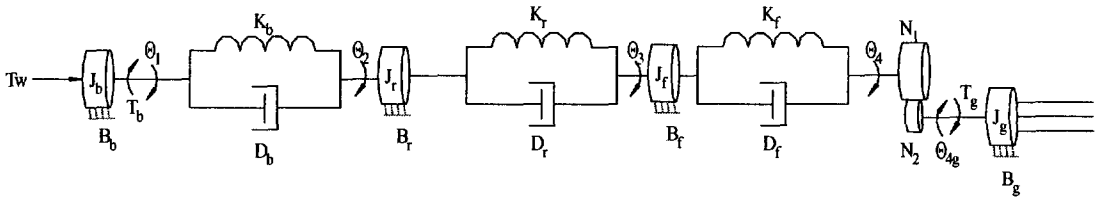

As noted above there are a number of simplifications to this model. The first simplification is that the three blades have been combined into a single rotational mass-spring-damper system. To make this simplification requires that the input torque provided by the wind be uniform over all three blades. It has been shown through previous experimentation that this is not actually the case, and that the wind speed will vary with heights above the ground. In the case of this model this factor is ignored and this thesis presents work on developing a control technique that controls the blade pitch angle for all three blades of the wind turbine simultaneously. The parameters for the gearbox are all lumped into the equivalent elements of the generator (rotational mass, spring and damping). For this thesis it is assumed that the properties of the hydraulic coupling fluid remain constant. This means that as the fluid heats up during normal operation, the fluid properties of damping and torsional spring will not change, meaning that the fluid is in a steady state condition. The model assumes steady state values for the damping and spring constant of the fluid drive. In addition to this assumption, for the PI and pole-placement controllers it is going to be assumed that the fluid coupler

solenoid is in a fixed position. This means that the solenoid valve within the fluid coupler will not be used as a means to provide any additional mitigation of torque variations on the drive train. The LQR controller developed in Chapter 4 makes use of the fact that the fluid drive coupling is not a fixed value and can be varied through a controllable bleeder valve to allow a constant torque to reach the gearbox, and it further decouples the torque variations provided by the rotor from the torque variations on the generator and gearbox.

The first step required in creating a control scheme for the simplified wind turbine shown in figure 2.1 is to generate the equations of motion for all the elements within the model. These equations are derived after reflecting the generator and its associated motions from the High Speed Shaft (HSS) to the Low Speed Shaft (LSS). The equivalent to doing this in an electrical system is to reflect the secondary side load of a transformer to the primary side to allow for the analysis of current flow and power losses. In the case of this mechanically rotating system, the speed of the generator is reflected back to the low speed shaft through the following equation:

$$\frac{1}{N} = \frac{\dot{\theta}_{LSS}}{\dot{\theta}_{HSS}} \tag{2.1}$$

In this equation $\dot{\theta}_{LSS}$ is the speed of the low speed shaft, $\dot{\theta}_{HSS}$is the speed of the high speed shaft, and N is the ratio of the gears. In this case N is assumed to take on a fixed gear ratio of 1:97, $N = \frac{1}{97}$. An ideal gearbox is assumed in this model. This assumption means for the purposes of modeling that the gearbox allows for

conservation of energy, and does not take into account losses due to friction or slipping of the gear teeth.

Since the model assumes an ideal gearbox, the following conservation of energy can be stated: power on the High Speed Shaft is equal to the power on the Low Speed Shaft. To find the mechanical power of a rotating shaft in watts, the following equation is used:

$$P = \dot{\theta} * T \tag{2.2}$$

In the above equation P is the power in watts; $\dot{\theta}$ is the rotational speed in radians per second; and T is torque in Newton meters (Nm). Because the model requires conservation of energy, equation 2.3 can be developed, by substituting in the results of equation 2.1 and solving for $\dot{\theta}_{HSS}$, equation 2.4 can be developed.

$$\dot{\theta}_{HSS} * T_{HSS} = \dot{\theta}_{LSS} * T_{LSS} \tag{2.3}$$

$$T_{LSS} = \frac{1}{N} * T_{HSS} \tag{2.4}$$

By using equation 2.4 the torques on the generator can be reflected on the left hand side of the gearbox.

$$T_{LSS} = \frac{1}{N}(J_g\ddot{\theta}_{4g} + B_g\dot{\theta}_{4g} + T_g) \tag{2.5}$$

In equation 2.5, J_g is the inertia of the generator, B_g is the friction on the generator, and $T_g$is the back torque on the generator provided by an electrical load. One additional substitution needs to be made to this equation to reflect all of the generator elements to the left hand side of the gearbox. This requires the use of

equations 2.2, 2.3 and 2.4. In these equations it is noted that the power of the system is related to the torque times the speed of the shaft. In the lossless gearbox $\dot{\theta}_{4g}$ and $\ddot{\theta}_{4g}$ must have their speeds adjusted by the factor $\frac{1}{N}$ to finish the translation of the generator to the LSS side of the gearbox. By making this substitution equation 2.5 becomes:

$$T_{LSS} = \frac{1}{N}(J_g * \frac{1}{N} * \ddot{\theta}_4 + B_g * \frac{1}{N} * \dot{\theta}_4 + T_g) \tag{2.6}$$

In equation 2.6 it should be noted that $\ddot{\theta}_4$ and $\dot{\theta}_4$ are the acceleration and velocity of the LSS.

With the generator torques now reflected onto the LSS, the equations of motion for the entire system can now be generated starting with the torque placed on the blades by the wind. By referring back to Figure 2.1 and equation 2.6 the following sets of equations of motion are realizable.

Equation 2.7 is the sum of the torque on the wind turbine blades. In this equation T_w is the torque applied to the blades by the wind, J_b is the inertia of the blades, B_b is the drag coefficient of the blades, D_b is the torsion damping of the blades, and K_b is the torsion spring of the blades. As noted previously equation 2.7 makes the assumption that the wind torque is uniform over the entire blade area, and that all the blades are lumped into a single rotating mass.

$$T_w = J_b\ddot{\theta}_1 + B_b\dot{\theta}_1 + D_b(\dot{\theta}_1 - \dot{\theta}_2) + K_b(\theta_1 - \theta_2) \tag{2.7}$$

In addition to the constant terms noted above, equation 2.7 also includes the following rotational acceleration, velocity and position terms: $\ddot{\theta}_1$ is the rotational acceleration of the blade tips, $\dot{\theta}_1$ is the rotational velocity of the blades, $(\dot{\theta}_1 - \dot{\theta}_2)$ is the difference in velocity between the blades and the rotor, and $(\theta_1 - \theta_2)$ is the difference in rotational position between the blades and the rotor. For specific reasons the differences between speeds and positions are listed in pairs. The primary reason for this is that the system shown in Figure 2.1 does not contain a free integrator. This will become important when the equations of motion are converted into state-space to allow for the creation of control algorithms. One step that is useful in aiding the conversion of the equations of motion into state-space is to turn the equations of motion into a standard form.

$$\ddot{X} = -B(x)\dot{X} - C(x)X + Q \tag{2.8}$$

Equation 2.8 represents a standard system solved for the acceleration acting on the body. Both B(x) and C(x) represent functions acting on the dissipative and spring elements of the system and Q represents the driving force of the system. Each of these elements has been normalized by dividing the equation through by the constant (mass in this case) associated with the acceleration term. Using equation 2.8 as the standard form, equation 2.7 can be re-written as follows:

$$\ddot{\theta}_1 = -\frac{B_b}{J_b}\dot{\theta}_1 - \frac{D_b}{J_b}(\dot{\theta}_1 - \dot{\theta}_2) - \frac{K_b}{J_b}(\theta_1 - \theta_2) + \frac{T_w}{J_b} \tag{2.9}$$

Moving from left to right in the simplified model, the next set of equations of motion are for the connection between the blades and the rotor. In this case there is not an external driving torque applied to the rotor, and all of the torque is supplied by the rotating blades.

$$D_b(\dot{\theta}_1 - \dot{\theta}_2) + K_b(\theta_1 - \theta_2) = J_r\ddot{\theta}_2 + B_r\dot{\theta}_2 + D_r(\dot{\theta}_2 - \dot{\theta}_3) + K_r(\theta_2 - \theta_3) \quad (2.10)$$

The important item to note about equation 2.10 is the change of sign on the driving forces from the blades. In equation 2.7 the D_b and K_b terms took on negative values, and as they become the driving elements of the rotor they take on positive values. This will occur throughout all of the derived equations of motion. Equation 2.10 contains the following additional rotational elements: J_r is the inertia of the rotor, B_r is the torsion damping of the rotor, and K_r is the torsion spring of the rotor. Putting this equation in standard form the following is obtained:

$$\ddot{\theta}_2 = \frac{D_b}{J_r}(\dot{\theta}_1 - \dot{\theta}_2) - \frac{K_b}{J_r}(\theta_1 - \theta_2) - \frac{B_r}{J_r}\dot{\theta}_2 - \frac{D_r}{J_r}(\dot{\theta}_2 - \dot{\theta}_3) - \frac{K_r}{J_r}(\theta_2 - \theta_3) \quad (2.11)$$

The following acceleration, velocity and position terms have been introduced in equations 2.10 and 2.11: $\ddot{\theta}_2$is the rotational acceleration of the rotor, $\dot{\theta}_2$is the rotational velocity of the rotor, $(\dot{\theta}_2 - \dot{\theta}_3)$ is the difference in velocity between the rotor and the fluid coupler, and $(\theta_2 - \theta_3)$ is the difference in rotational position between the rotor and the fluid coupler.

The equation of motion for the fluid coupler is as shown in equation 2.12,

$$D_r(\dot{\theta}_2 - \dot{\theta}_3) + K_r(\theta_2 - \theta_3) = J_f\ddot{\theta}_3 + B_f\dot{\theta}_3 + D_f(\dot{\theta}_3 - \dot{\theta}_4) + K_f(\theta_3 - \theta_4) \quad (2.12)$$

where J_f is the inertia of the fluid, B_f is the rotational friction of the fluid, D_f is the damping constant of the fluid, and K_f is the rotational spring constant of the fluid. Putting this equation in standard form results in:

$$\ddot{\theta}_3 = \frac{D_r}{J_f}(\dot{\theta}_3 - \dot{\theta}_2) - \frac{K_r}{J_f}(\theta_3 - \theta_2) - \frac{B_f}{J_f}\dot{\theta}_3 - \frac{D_f}{J_f}(\dot{\theta}_3 - \dot{\theta}_4) - \frac{K_f}{J_f}(\theta_3 - \theta_4) \tag{2.13}$$

Equations 2.12 and 2.13 include the following rotational motion elements: $\ddot{\theta}_3$is the rotational acceleration of the fluid, $\dot{\theta}_2$is the rotational velocity of the fluid, $(\dot{\theta}_3 - \dot{\theta}_4)$ is the difference in velocity between the fluid coupler and the gearbox, and $(\theta_3 - \theta_4)$ is the difference in rotational position between the fluid coupler and the gearbox.

As noted in equation 2.6 above, the generator and its associated rotational elements need to be translated to the left hand side of the gearbox to enable an analysis of the system. With this translation made the equation of motion between the fluid coupler and the gearbox can be developed as follows:

$$N^2 D_f(\dot{\theta}_3 - \dot{\theta}_4) + N^2 K_f(\theta_3 - \theta_4) = J_g\ddot{\theta}_4 + B_g\dot{\theta}_4 \tag{2.14}$$

One of the items that can be noted is that the term for the constant back torque on the generator has been removed. The reasoning behind this is to allow for creation of the advanced control systems discussed in chapters 3 and 4. For this system the back torque noted in 2.6 will be incorporated into the model in the generator friction term. The reasoning behind this is that the actual value of the generator friction is actually extremely small when compared to the units of the rest of the system. By equating this

back friction term to the back generator torque the external input can be removed from the equation. It has been shown through previous experiments that the back torque of the generator is nearly constant when held in a tight speed operating range. Instead of making the torque a non-linear function, it is normally modeled as a constant for simplicity. (10) Thus equation 2.14 can then be realized in standard form as:

$$\ddot{\theta}_4 = -\frac{B_g}{J_g}\dot{\theta}_4 - \frac{D_f * N^2}{J_g}(\dot{\theta}_3 - \dot{\theta}_4) - \frac{K_b * N^2}{J_b}(\theta_3 - \theta_4) \tag{2.15}$$

With all of the equations of motion derived, equations 2.9, 2.11, 2.13 and 2.15 can be realized in a Simulink® model. Simulink® is a graphical modeling tool that is an add-on to the MATLAB® program developed by Mathworks™. In the Simulink® interface all of the constants and integrators derived above can be put into block diagram form to allow for easy analysis of the individual components of the system. When this is combined with an M-file developed in the MATLAB interface, gain variables can be included in the Simulink® model and these variables can be easily changed in the M-file text instead of through the graphical interface. The model for the system developed above is shown in figure 2.2.

Figure 2.2 – Simplified Wind Turbine With Fluid Coupler Block Diagram

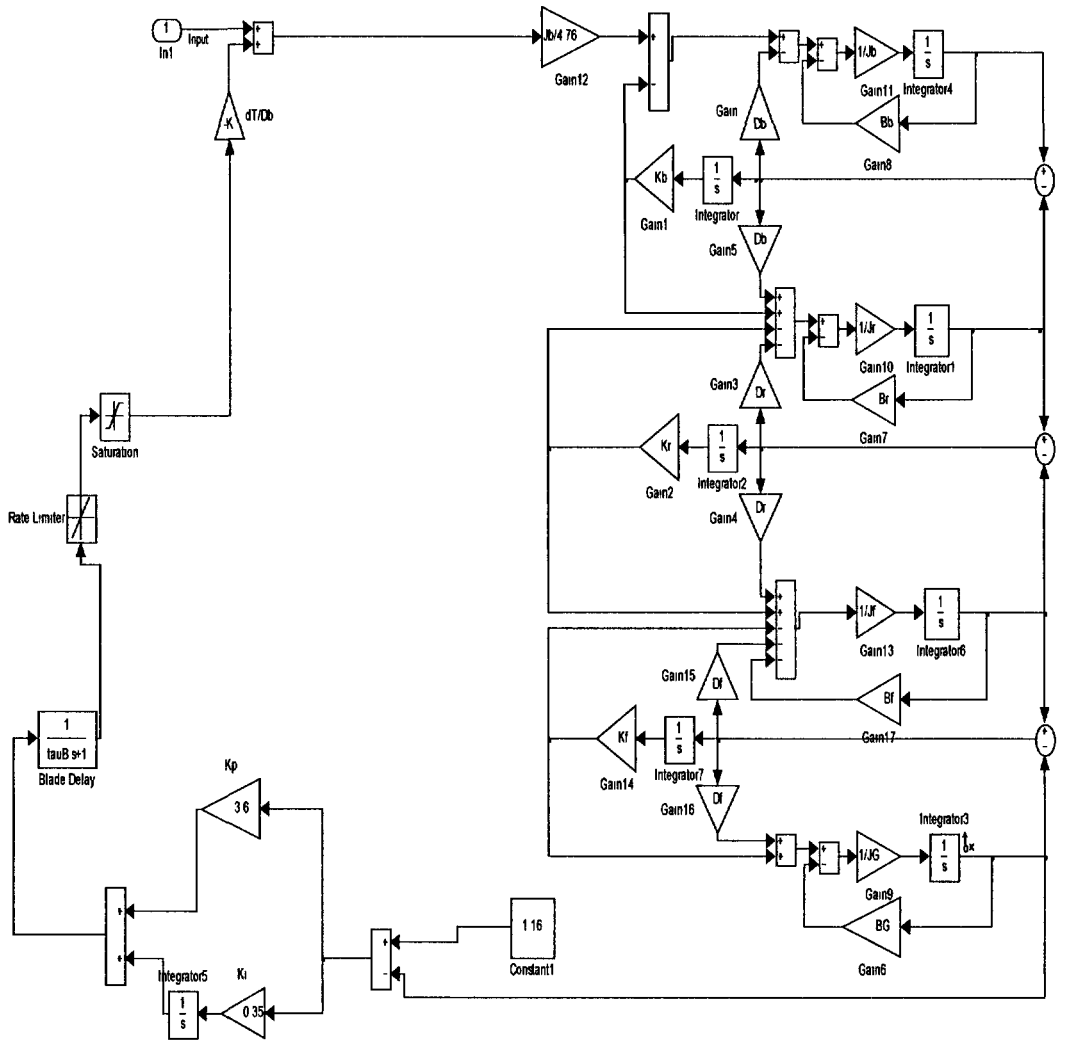

System Model Parameters

The system shown in Figure 2.2 and in the equations of motion developed above contains a number of different constants. The majority of these have been developed through the NREL FAST model of a 5 MW wind turbine, and specific values for the blade

damping coefficient and the blade drag coefficient (B_b, D_b) were developed by Jacob Aho for this linear model (9), (11). The values of the variables used in this model can be found in Table 2.1 below.

Table 2.1 – Wind Turbine Parameters and Values

Variable Name	Symbol	Value	Units
Mass all 3 Blades	M_b	5.32E+04	kg
Inertia all 3 blades	J_b	3.53E+07	kg-m^2
Blade Drag Constant	B_b	0	Nm/(rad/sec)
Blade Damping coefficient	D_b	1.41E+08	Nm/(rad/sec)
Blade Spring Constant	K_b	2.82E+08	Nm/rad
Inertia of the Rotor	J_r	1.15E+05	kg-m^2
Rotor Friction Loss	B_r	11000	Nm/(rad/sec)
Rotor Torsion Damping	D_r	6.22E+06	Nm/(rad/sec)
Rotor Spring constant	K_r	8.68E+08	Nm/rad
Fluid Inertia	J_f	13200	kg-m^2
Laminar Fluid Losses	B_f	66000	Nm/(rad/sec)
Fluid Damping Coefficient	D_f	7.46E+07	Nm/(rad/sec)
Fluid Spring Constant	K_f	800	Nm/rad
Generator Inertia	J_g	5.34E+02	kg-m^2
Equivalent Friction Drag on Generator	B_f	330.98	Nm/(rad/sec)
Rated Output Power	P_o	5,000,000	Watts
Blade actuator time constant	τ_b	0.2	Secs
Fluid coupler time constant	τ_f	0.25	mSecs
Gear Ratio	N	97	

Sources: (9) & (11)

The values for the fluid coupler were found through model experimentation or from general characteristics of a fluid coupler. The first value that was derived was the fluid coupling loss or laminar fluid flow. This value is calculated through the typical data provided by Peerless on one of their fluid coupling pumps (12). In this datasheet they provide that the 3-time constant value for a zero to full power step transition is 15 seconds. By using a simple first order system, as shown below in Figure 2.3, the time constant can be equated into a value for the pump loss elements.

Figure 2.3 – First Order Linear Pump Loss Model

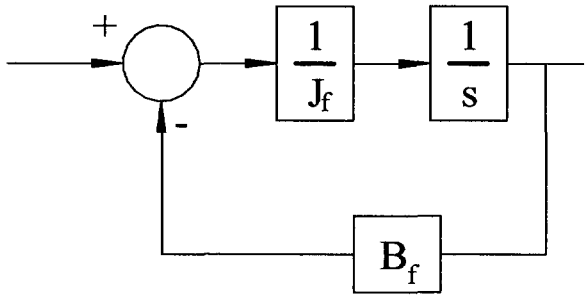

Based on using three time constants to reach the system steady-state value for the pump, the following equation can be developed for the pump values:

$$TF = \frac{\frac{1}{J_f * s}}{1 + \frac{B_f}{J_f * s}} = \frac{\frac{1}{J_f}}{s + \frac{B_f}{J_f}} \tag{2.16}$$

$$\tau = 5 = \frac{J_f}{B_f} \tag{2.17}$$

The inertia of the fluid is estimated based on the following assumptions. First the weight of a 5 MW fluid coupling drive is 33000 kg (13). Based on the weight of the coupler, it is assumed that 55% of the weight is directly related to the coupler housing and cooling systems, which leaves the remaining 45% of the weight to be dedicated to the moving fluid and physically moving pump/coupler components. For further ease of calculation, the fluid coupler is assumed to have a transfer efficiency of 95%. Similar fluid couplers advertise efficiencies between 93 – 97%. Furthermore, the radius of the fluid coupling drive is assumed to be 1.414 m, and the coupler is viewed as a solid disk. By using these assumptions, the inertia of the fluid coupler can be found from:

$$J_f = \frac{1}{2} m * r^2 \tag{2.18}$$

As can be seen from equation 2.18, the value for the radius of the rotating fluid was selected to allow $J_f = m$, which in this case is taken to be 0.45 * total mass of the fluid coupler.

These values for J_f and B_f were plugged into the derived linear model of the wind turbine as shown in Figure 2.1. An assumption was then made for how the fluid coupler would transfer energy from the rotor to the gearbox. It was assumed that majority of the rotational energy would be transferred to the gearbox through the damping element of the fluid. This assumption is based on the idea that the fluid coupler is going to transmit a constant torque and buffer the springiness of the system. The fluid still contains a spring element as a hydraulic fluid under high pressure cannot act strictly as a buffering agent.

Based on these assumptions, the Simulink® model was run open loop with a constant input of 1 representing a constant wind speed of 18 m/s. The values of D_f and K_f were arrived at through an iterative process. As stated above the fluid coupler was assumed to operate at 95% efficiency, which was taken as allowing the gearbox speed to fall to 95% of its rated speed, and D_f was made the dominant element of the power transfer. Based on these requirements the values of D_f and K_f were found to be 74.64E6 Nm/(rad/s) and 800 Nm/rad respectively.

Wind Speed Input Model Simplification

The model shown in figure 2.1 contains one further simplification that needs to be discussed. In the model the input to the blades is scaled by a constant factor of:

$$\frac{J_b}{4.76}$$

This represents a change to the previously derived models of this system, and deserves some additional explanation on how this value was determined.

In the previous system models, such as those developed by NREL and Jake Aho, the input model of the wind speed, blade pitch and rotor shaft speed interactions were all added together and then used to drive the blades. The previous model representation is shown in Figure 2.4.

Figure 2.4 – Wind Turbine, Torque Input Model

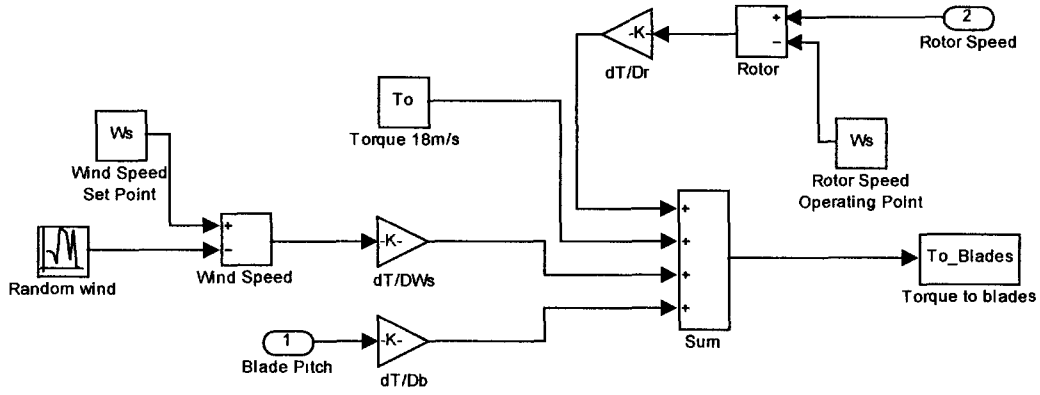

Source: (9)

In order to validate the new input model developed for this thesis, the original system model, without the fluid coupler, was run open loop with a constant input, and the wind speed was normalized to a value of one. A gain was then placed between the normalized input and the blades, and its value was iterated until the output with a constant input matched that of the system that included the torque model shown above. By doing these iterations the model is able to be reduced from the system shown in Figure 2.4 to that of a single factor where the inertia of the blades is divided by a constant factor of 4.76.

In order to further establish the validity of this single gain model as compared to the structure in shown in Figure 2.4, each of the systems was run closed loop with a step input in the wind speed. The blade pitch responses of each system and the generator shaft speeds were then compared. Because the blade pitches and generator speeds of

each of the systems were shown to be within 2% of each other, it was decided to use the single gain element model for the input to the wind turbine.

PI Controller Development

As the system shown in Figure 2.1 does not have an industry standard controller to which any derived results may be compared, an industry standard controller of proportional-integral (PI) type must be developed to allow for a base-line comparison for the advanced controllers developed in Chapters 3 and 4. At the time of writing this thesis, the wind turbine industry is standardized on PI control for the blade pitch control mechanism. There are a number of reasons for this choice including the fact that this becomes a single stage controller with only two sets of gains to find. Also, because the system is controlled only from a single output, the generator speed, there is not the need to add numerous other measurement devices and the wiring to provide feedback from all of the other states within the system. One of the other driving forces behind the use of PI controllers is that they are very common and easy for control engineers to trouble shoot.

As a start for developing a PI controller for the current model, the system was run under an open loop condition with a step input of 1. The purpose of running the system open loop was to determine the settling time of the open loop system. As can be seen from figure 2.5, the open loop system responds to a step function with a settling time of approximately 40 seconds with no overshoot. It should be noted that in

the figure below the wind speed has been normalized to 18 m/s, and the step input represents a change in wind speed of 1 m/s.

Figure 2.5 – Open Loop System Response to a Step Input

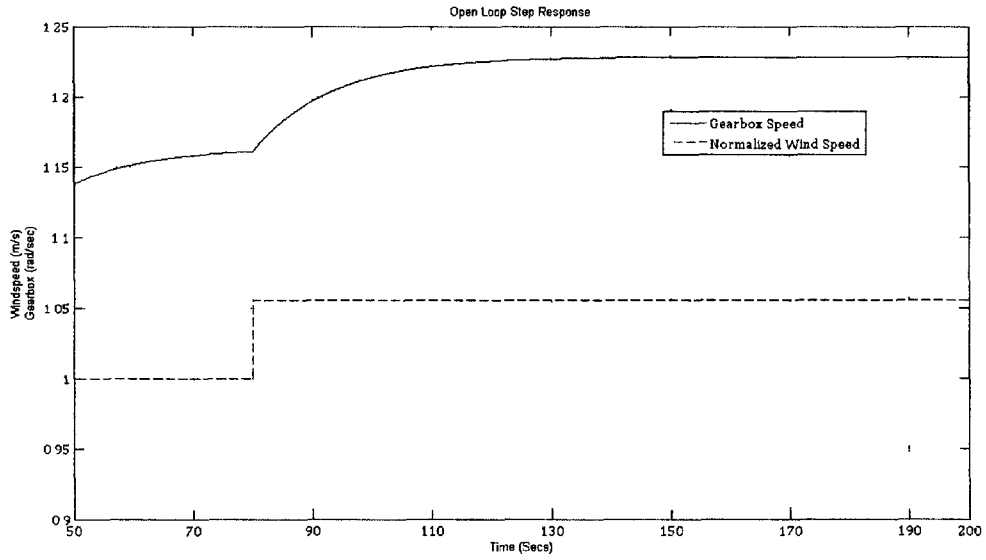

Based on the response of the system, the following parameters were chosen to be the development criteria for the closed loop system: Settling Time = 10 seconds, and percent overshoot = 10%. Of these two performance criteria the percent overshoot is the dominant criterion as the system can be allowed to come up to speed more slowly as long as the generator shaft speed (HSS) does not exceed the rated speed for the generator. Ideally, this design parameter would include additional headroom of 10% to allow for modeling errors and component tolerances. This thesis assumes that the generator manufacturer has already included additional headroom in the rated speed specification, so no additional derating of the system is required prior to developing the control algorithm.

Based on the analysis performed by the NREL on the Repower 5 MW machine, the proportional and integral gains of the controller should have a ratio of approximately 3:1 (11). This became the baseline for creating the controller gains of the system with the fluid coupler in-line. The additional constraint on the controller is that proportional (K_p) and integral (K_i) gains must be kept small so that the controller allows the wind turbine blades to pitch slowly and does not create other unaccounted resonances within the machine. Using all these criteria and the NREL gain schedule as a starting point, the following gains for K_p and K_i were found by testing in the model through an iterative process and implemented into the system block diagram as shown in Figure 2.6.

Figure 2.6 – PI Controller Implementation

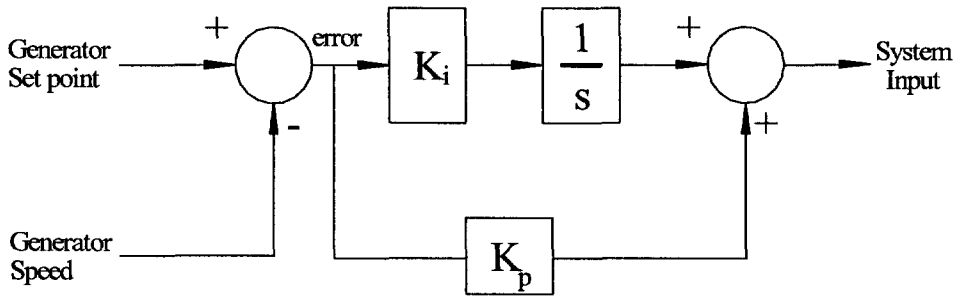

Given the values that were found for K_p and K_i, the system Bode plot and Nyquist plot were generated to show the frequency response at the linearization point of the system. In this case the linearization point is taken as an input wind speed of 18 m/s and a starting blade-pitch angle of 15.98°. Analysis of the Bode and Nyquist plots allow for the gain and phase margins of the system to be determined, and also allow for the system stability to be stated.

Figure 2.7 – Open Loop Bode Plot of PI Controller and Wind Turbine Model

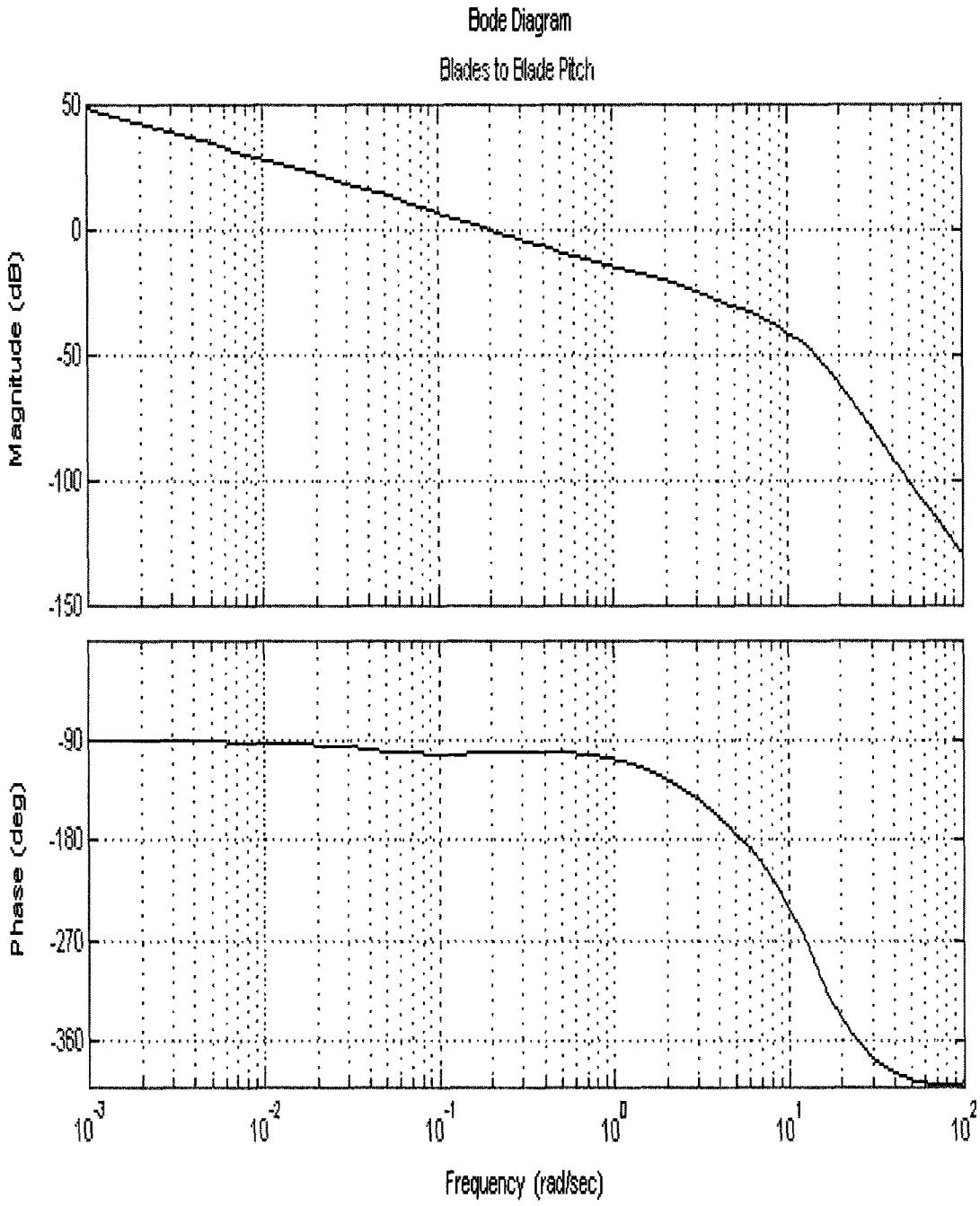

Based on a review of the Bode plot of the open loop system, the gain and phase margin of the system can be found. The phase margin is described by the phase difference between the system and -180° when the overall gain of the system is equal to

0 db. From reading the Bode plots above this value is 87°. Using a similar set of criteria the gain margin of the system can be found. The gain margin is the difference between the system gain and 0 db when the phase is 0°. In this case the gain margin is 28 db (14). One of the interesting items to note on this plot is that the 0 db point is at approximately 0.3 Hz. This means that the system is attenuating the amplitudes of any frequency above this point. In addition it can be seen that the gain continues to fall off at about 40 db per decade, and does not have a secondary resonant peak. A comparison of this plot with those that have been derived for the FAST model and the linear model without the fluid coupler shows that the addition of this damping element, the fluid coupler, removes a resonant frequency at approximately 1.5 Hz [(9) , (11)]. This is significant in the fact that just the addition of the fluid coupler has changed the open loop system from an under-damped resonant system to an over-damped system.

The same information that was found via the Bode plots in Figure 2.7 can also be found by reviewing the Nyquist plot of the system. On the Nyquist plot the gain margin is the distance away from the -1+j0 point where the system crosses the real-imaginary axis defined as 1/a. The phase margin of the system is the angular distance away from the negative real axis when the magnitude of the system gain is 1 (15). Bode plots will be used to show stability criteria of the two advanced controllers developed in chapters 3 and 4.

Figure 2.8 – Open Loop Nyquist Plot of PI Controller and Wind Turbine Model

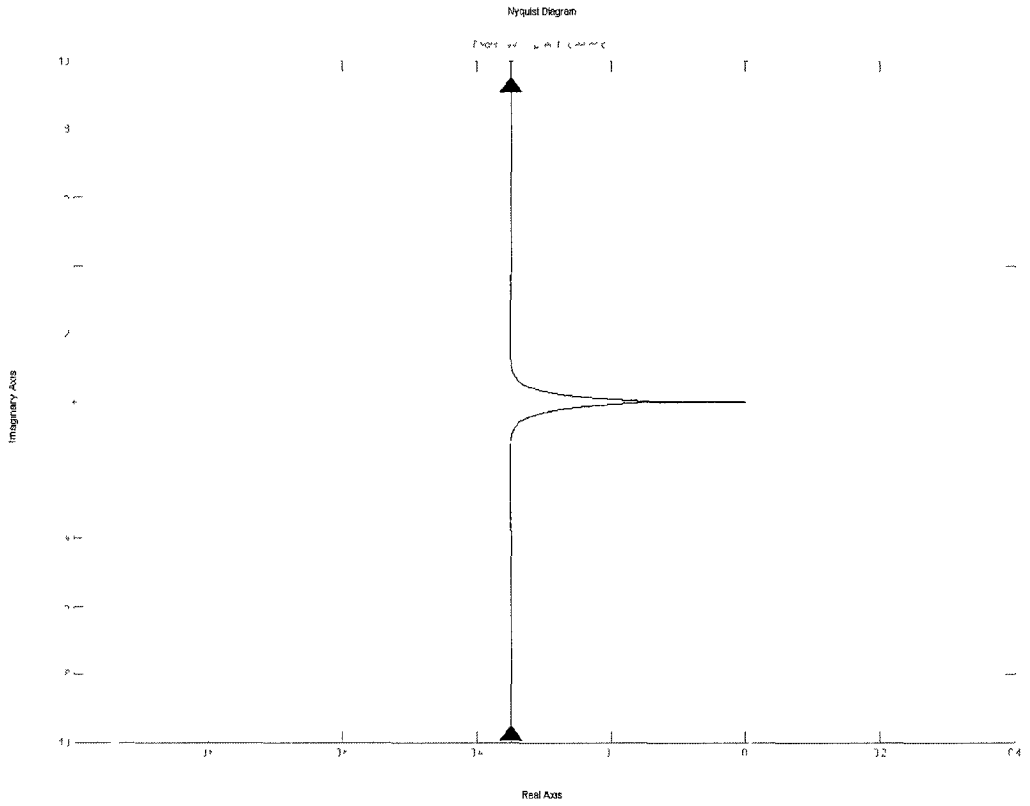

Based on Figures 2.7 and 2.8, it can be seen that the system is stable open loop. The desired design criteria to hold a stable system is for a minimum phase margin of 45° and a minimum gain margin of 6 db. Because the model's open loop gain and phase margins are far enough away from the minimum values, it can be concluded that the system will be stable even with manufacturing tolerances and modeling inadequacies.

The closed-loop plot of the PI controller with the same step excitation as in figure 2.5 is shown in Figure 2.9. As noted previously, the design goal for this controller was a settling time of 10 seconds and a maximum overshoot of 10%. A review of figure 2.9 shows that the desired results have been achieved. The only item left to determine

is if reasonable numbers for the proportional and integral controller elements have resulted in reasonable numbers for the blade pitch. As before, the wind speed has been normalized to 18 m/s.

Figure 2.9 – Closed-Loop PI Control Step Response

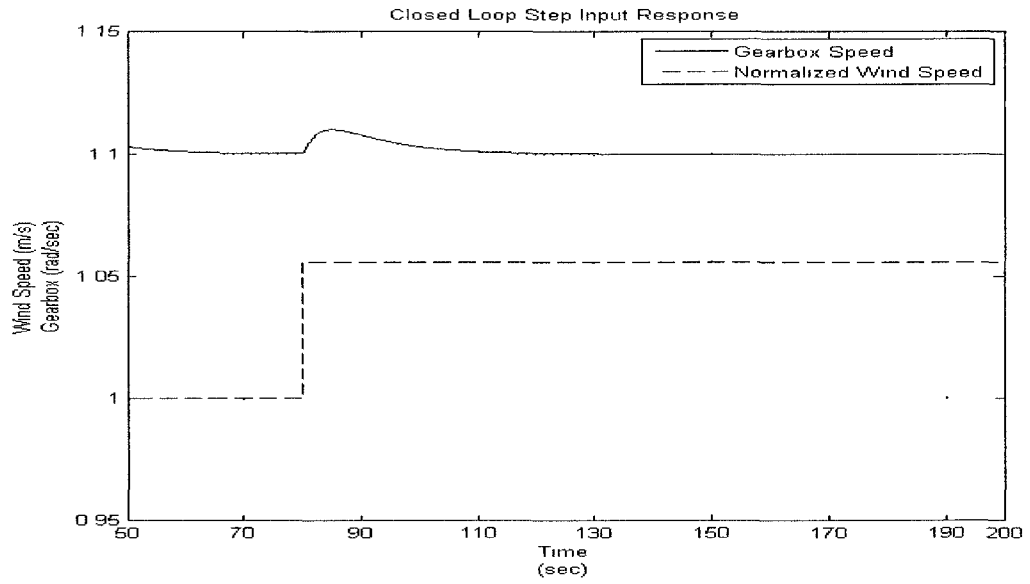

PI Controller Verification

Because there is not an established model for a large wind turbine with a fluid coupling drive, there is not a baseline system to test the model and controller validity against. This leads to the question of how well the PI controller is working compared to a known system. In order to evaluate the PI controller developed in this thesis, the system was compared to the derived linear model developed by Jacob Aho (9). Each of the systems were run assuming a constant wind speed of 18 m/s and a white noise input with a variance of 0.38 m/s^2. Based on these input conditions, the error signals from the

PI controllers and the output speeds of the generators were compared. The desired characteristic is that the error signal of the fluid coupler model is equal to or smaller than the error signal from the model without the fluid coupler. In addition to this goal the two generator speeds are desired to be at the same value with a minimal phase shift between them. The results of the system comparison are shown below in Figure 2.10. The graph in Figure 2.10 shows the two error signals that from driving each of the systems with the same random wind speed.

Figure 2.10 – Closed Loop PI Controller Parameter Comparison

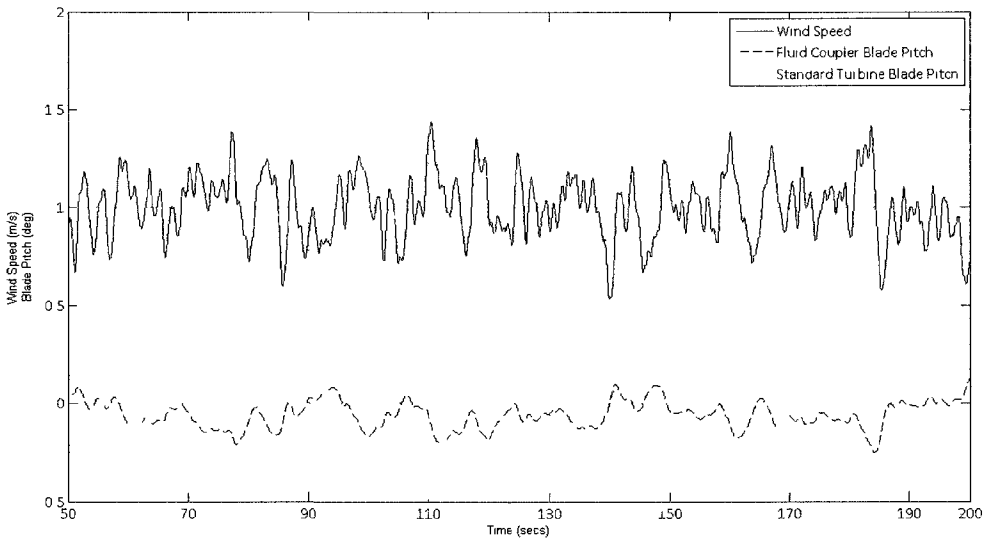

As the graphs in Figure 2.10 show, the error signals of the two controllers are within 10% of each other. Given this fact, it can be concluded that the PI controller for the fluid coupled output is an adequate baseline design as it has been previously shown that the model without the fluid coupler has a maximum blade slew rate of 2.2°/sec when driven with a wind file with a similar power spectral density. Because the two

controllers result in a similar amount of blade pitch error the PI Controller developed in this section will be used as the baseline comparison for the advanced controllers (pole-placement and LQR) developed in chapters 3 and 4. All of the simulation results and comparisons between the three controllers will be discussed in Chapter 5.

CHAPTER 3:

POLE-PLACEMENT CONTROLLER

Reasons for Advanced Controller Development

As can be seen in the previous chapter, a PI controller can provide a robust control algorithm, but it is not without its disadvantages. One of the biggest drawbacks of using a PI controller is that it is always late. In terms of the wind turbine system, that means that by the time the controller is able to react to a change of wind speed that reaches the generator, the torque change has already reached and passed through the gearbox. Because of this the PI controller can provide some protection to the system, but it would be able to do a better job if it had advanced knowledge of what was happening to the system. In other words the controller should be better able to mitigate torque variations caused by changes in the wind if it has information about the other states of the system. There are two different controller options/controller design techniques that can be used to accomplish this goal. The first option is Pole-Placement, in which all the system states are fed back and are assigned new pole locations that are typically faster and less oscillatory. The second option, which will be discussed in Chapter 4, is a Linear Quadratic Regulator (LQR), which assigns penalties to each of the states to calculate the optimal gains for each state.

In either case the more advanced controllers require knowledge of all of the states of the system, and these can be provided for either through additional sensors or through a combination of state estimators and sensors. The state estimator can either be a model developed by selecting pole location that are approximately 10 x faster than the original poles or the state estimator can be modeled through Kalman filtering. For the purpose of this thesis it is assumed that all of the state data is available directly through sensors in the various elements within the turbine. For example, resistive strain gauges can be placed in the blades to provide spring data, and tachometers can be placed on each of the rotating elements to provide data for each of those states. In addition to these data the current system has clean encoder measurements of the generator speed, so the creation of observers is a simple task. The development of state estimators and Kalman filtering for this system is not included in this work, but these ideas would be something to consider in the future.

Pole Placement and State Designations

The pole-placement design technique allows the control designer to select the eigenvalues of the closed-loop system to meet desired performance parameters. This technique can be conceptually simpler to use than the LQR, or optimal control method because pole locations are chosen rather than applying penalties on each of the states. The drawback of this technique is determining which poles are associated with particular states within the system. In larger systems this leads to a large number of

pole locations that will have to be selected and tested via simulation. There is also no guarantee with pole-placement that you will be able to maintain an acceptable gain and phase margin or stay within the maximum slew rate of the blades.

The pole-placement technique begins by placing the system in state-space form. As stated in Chapter 2, for this wind turbine system the equations of motion can lead to a system with a free integrator. For that reason the states of the system should be selected from the block diagram and not directly from equations 2.9, 2.11, 2.13 and 2.15. Figure 3.1 below defines each of the states of the system and allows the creation of a standard form of:

$$\underline{\dot{x}} = \underline{A} * \underline{x} + \underline{B} * \underline{u} \tag{3.1}$$

$$\underline{y} = \underline{C} * \underline{x} + \underline{D} * \underline{u}$$

Figure 3.1 – State Space Variable Definition

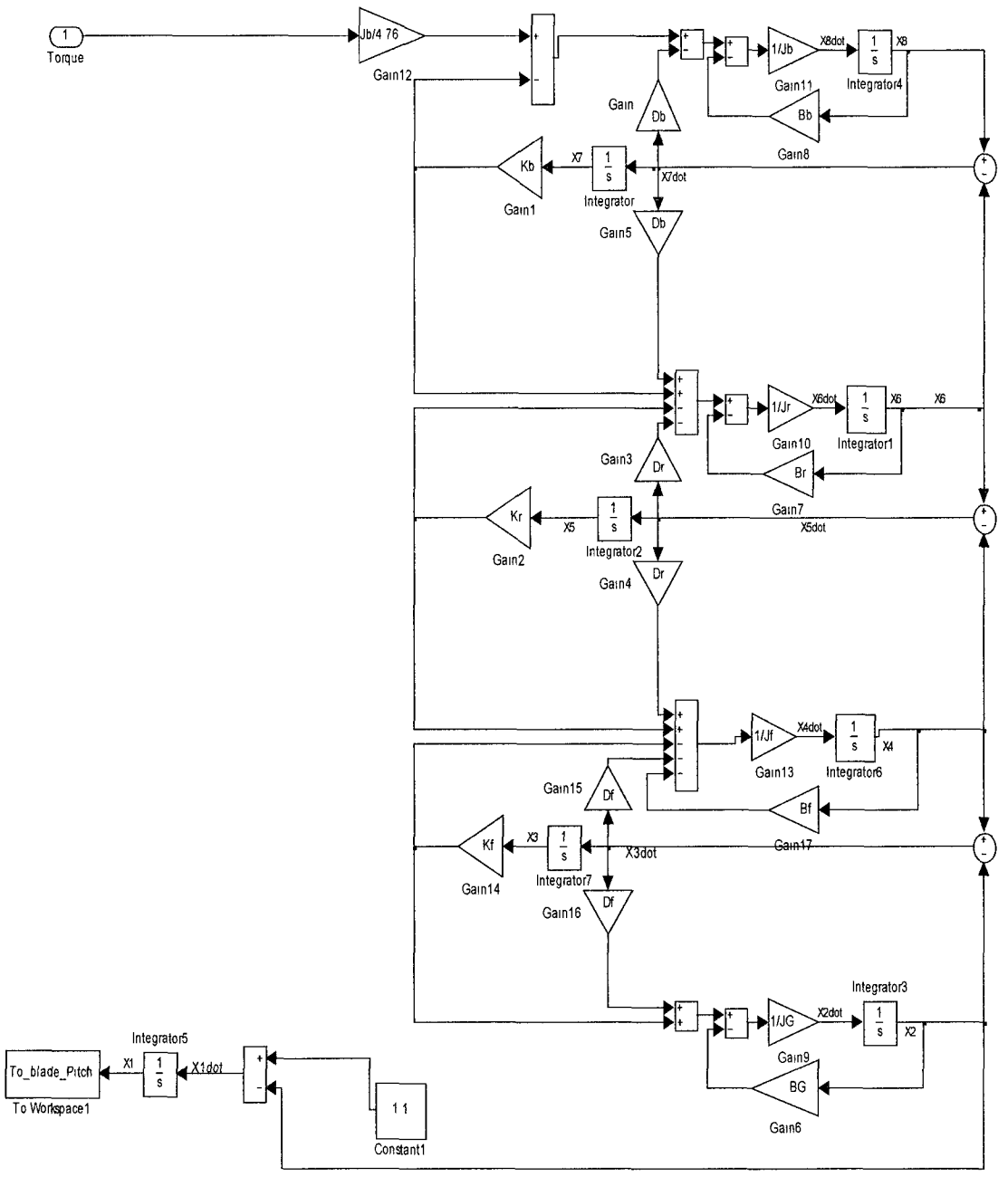

Using the block diagram the following matrices can be developed to describe the system:

$$\underline{\dot{x}} = \begin{pmatrix} \ddot{\theta}_4 \\ (\dot{\theta}_3 - \dot{\theta}_4) \\ \ddot{\theta}_3 \\ (\dot{\theta}_2 - \dot{\theta}_3) \\ \ddot{\theta}_2 \\ (\dot{\theta}_1 - \dot{\theta}_2) \\ \ddot{\theta}_1 \end{pmatrix}, \quad \underline{x} = \begin{pmatrix} \dot{\theta}_4 \\ (\theta_3 - \theta_4) \\ \dot{\theta}_3 \\ (\theta_2 - \theta_3) \\ \dot{\theta}_2 \\ (\theta_1 - \theta_2) \\ \dot{\theta}_1 \end{pmatrix} \tag{3.2}$$

$$\underline{A} = \begin{pmatrix} -\frac{B_g + D_f}{J_g} & \frac{N^2 * K_f}{J_g} & \frac{N^2 * D_f}{J_g} & 0 & 0 & 0 & 0 \\ -1 & 0 & 1 & 0 & 0 & 0 & 0 \\ \frac{D_f}{J_f} & -\frac{K_f}{J_f} & -\frac{D_r + D_f + B_f}{J_f} & \frac{K_r}{J_f} & \frac{D_r}{J_f} & 0 & 0 \\ 0 & 0 & -1 & 0 & 1 & 0 & 0 \\ 0 & 0 & \frac{D_r}{J_r} & -\frac{K_r}{J_r} & -\frac{D_r + D_b + B_r}{J_r} & \frac{K_b}{J_r} & \frac{D_b}{J_r} \\ 0 & 0 & 0 & 0 & -1 & 0 & 1 \\ 0 & 0 & 0 & 0 & \frac{D_b}{J_b} & -\frac{K_b}{J_b} & -\frac{B_b + D_b}{J_r} \end{pmatrix}$$

$$\underline{B} = \begin{pmatrix} 0 & 0 & 0 & 0 & 0 & 0 & \frac{J_b}{4.76} \end{pmatrix}^T, \quad \underline{C} = (1 \quad 0 \quad 0 \quad 0 \quad 0 \quad 0 \quad 0) \tag{3.3}$$

It should be noted that the $\underline{D}$ matrix is omitted from the system shown in equation 3.3. This is due to the fact that the $\underline{D}$ matrix is a $\underline{0}$ matrix as there are no direct contributions from the system input to the system output. From the system state space matrices

developed above, it can be seen that the system is a type zero system and cannot track a step response with no steady state error. Because of this the system matrices need to be augmented to force the system to be a type 1 system. The system matrices are augmented as shown in equation 3.4 (15).

$$\underline{A_a} = \begin{pmatrix} 0 & -C \\ 0 & \underline{A} \end{pmatrix}, \underline{B_a} = \begin{pmatrix} 0 & \underline{B} \end{pmatrix}^T \tag{3.4}$$

The augmented matrices $\underline{A_a}$ and $\underline{B_a}$ are used to develop the control system parameters for the pole placement algorithm.

One of the items that has to be checked before the pole-placement or optimal control state feedback techniques can be used is the controllability matrix of the system. The controllability matrix lets the designer determine whether or not all the states can be affected by a change in input. It will also give insight to the designer as to whether or not any of the states of the system are linearly coupled together. The controllability matrix is given by the following (15):

$$\underline{C_n} = \begin{bmatrix} \underline{B} & \underline{AB} & \underline{A^2B} & \cdots & \underline{A^{n-1}B} \end{bmatrix} \tag{3.5}$$

In order for the system to be fully controllable the rank of $\underline{C_n}$ must be full. This means that the matrix has an inverse, and that none of the rows/columns are linear combinations of each other. In the case of the wind turbine system the controllability matrix would be tedious to calculate by hand since the A matrix has seven rows and columns. MATLAB™ will be used to create this matrix through the code "ctrb" and then

the rank of the controllability matrix can be calculated and an evaluation can be done to ensure that the controllability matrix is of full rank.

The first step in the algorithm is to find the original system eigenvalues. These are found via the characteristic equation of the system (16), (15):

$$\left|\Lambda \underline{I} - \underline{A_a}\right| = 0 \tag{3.6}$$

The next step is to choose the locations of the new poles to operate the system. In order for the chosen pole locations to work, the system must be controllable. As long as the system is controllable the poles can be arbitrarily chosen so that the pole locations move to the left and closer to the jw axis to make the system faster and less oscillatory. The system feedback from the pole placement is given by (16):

$$\underline{u} = -\underline{K} * \underline{x} \tag{3.7}$$

In equation 3.6, $\underline{K}$ is a 1 x n matrix that gives the gains for each of the system states. By using the desired feedback law above, the closed loop system equation becomes:

$$\dot{\underline{x}} = \left(\underline{A_a} - \underline{B_a} * \underline{K}\right)\underline{x} + \underline{B_a} * \underline{u} \tag{3.8}$$

The new eigenvalues of the system, which are the chosen pole locations, are then given by:

$$\left|\Lambda \underline{I} - \underline{A_a} + \underline{B_a} * \underline{K}\right| = 0 \tag{3.9}$$

The values of $\underline{K}$ can be found by solving the simultaneous equations resulting from equation 3.8. While this can be done by hand for second and third order systems, the

calculations can get tedious to find each of the individual $\underline{K}$ elements for greater values of state size n. The code to solve all of these simultaneous equations is contained within the MATLAB™ program through the command "place".

To begin the pole-placement routine for the system shown in figure 3.1, the eigenvalues of the open loop system must be found using equation 3.6. Rather than solving this equation by hand, the "eig" function within MATLAB™ will be used. The open loop eigenvalues of the system are:

$$\Lambda_i = -6129, -7.1 \pm 12.5j, -12, -2.4, -0.0763, -1.076E-5, 0 \qquad (3.10)$$

By looking at the eigenvalues above, it can be seen that there is one very fast mode located to the left of -6000, and a number of other poles located close to the origin, including one pair of oscillatory poles. The poles located close to the origin are the dominant system poles, and these are the poles that need to be moved to affect the system response. To start the placement routine, the pole values for the smaller poles will be selected to be about 10% larger, and about 10% less oscillatory. The one pole that will be selected to move further is the pole located at the origin due to the integrator to make the system a type 1. This pole will be moved to approximately -2 so that the error response will be reduced as quickly as possible without overdriving the system.

All of the poles of the system are selected through an iterative process in which the closed loop response of the system is adjusted to match the desired criteria. From chapter 2 the baseline performance criteria for the system is to come up to speed in 10 seconds with no more than 10% overshoot given a step input of 1. By running through

multiple iterations for the pole locations, the following pole locations were found to provide the desired system response.

Selected pole locations:

$$P = -1.094E + 7, 8.0 \pm 10j, -6129.5, -18, -0.20, -1.07E - 5, -2.05 \quad (3.11)$$

From these selected pole locations, equation 3.9 can be used to calculate the feedback gains of all of the states of the system. Table 3.1 shows each of the calculated feedback gains and the states to which they are associated.

Table 3.1 – Pole-Placement State Feedback Gains

Feedback Gains		Associated State	Description
k_1	-1.4114	e	Gain on the integrated gearbox speed error
k_2	1.0780	$\dot{\theta}_4$	Gain on the gearbox speed error
k_3	0.0563	$(\theta_3 - \theta_4)$	Gain on the difference between the output fluid coupler and the gearbox shaft
k_4	-2.4693	$\dot{\theta}_3$	Gain on the fluid coupler speed error
k_5	20.2960	$(\theta_2 - \theta_3)$	Gain on the difference between the rotor position and the input fluid coupler position
k_6	5.3155	$\dot{\theta}_2$	Gain on the rotor speed error
k_7	4.9997	$(\theta_1 - \theta_2)$	Gain on the difference between blade and rotor position
k_8	2.9507	$\dot{\theta}_1$	Gain on the blade speed error

Each of the feedback gains associated with the desired pole locations is implemented in the wind turbine model as shown in Figure 3.2. One of the items shown in Figure 3.2 that has not been previously discussed is the three cascaded transfer functions attached to the random number generator. These transfer functions create the filter for the random wind speed. The creation of the random wind input will be discussed further in Chapter 5.

Figure 3.2 – Pole-Placement Feedback Data Flow

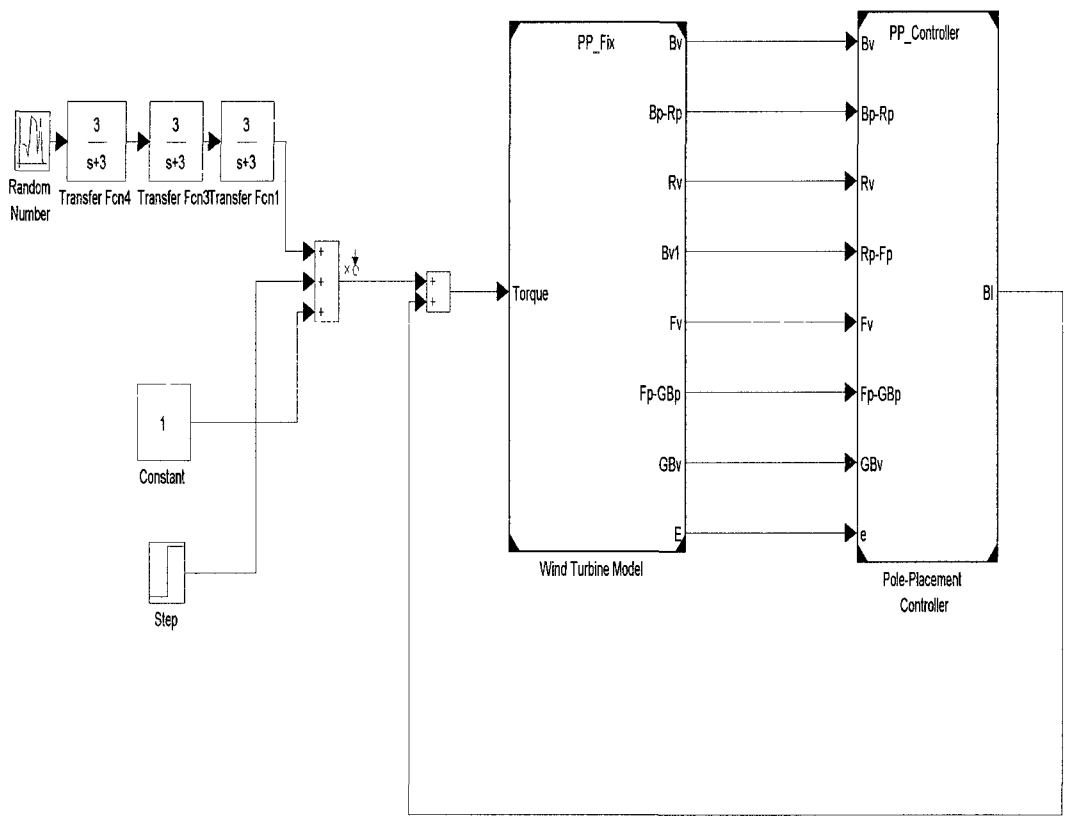

One of the drawbacks of using pole placement is that the stability and phase margin of the system are not guaranteed by design. This means that after having selected the desired pole locations the system Bode plots need to be reviewed to make sure that the minimum desired phase and gain margins are maintained. For the poles selected above in 3.11 the system has the following gain and phase plots:

Figure 3.3 – Closed loop Bode Plot Pole-Placement Controller

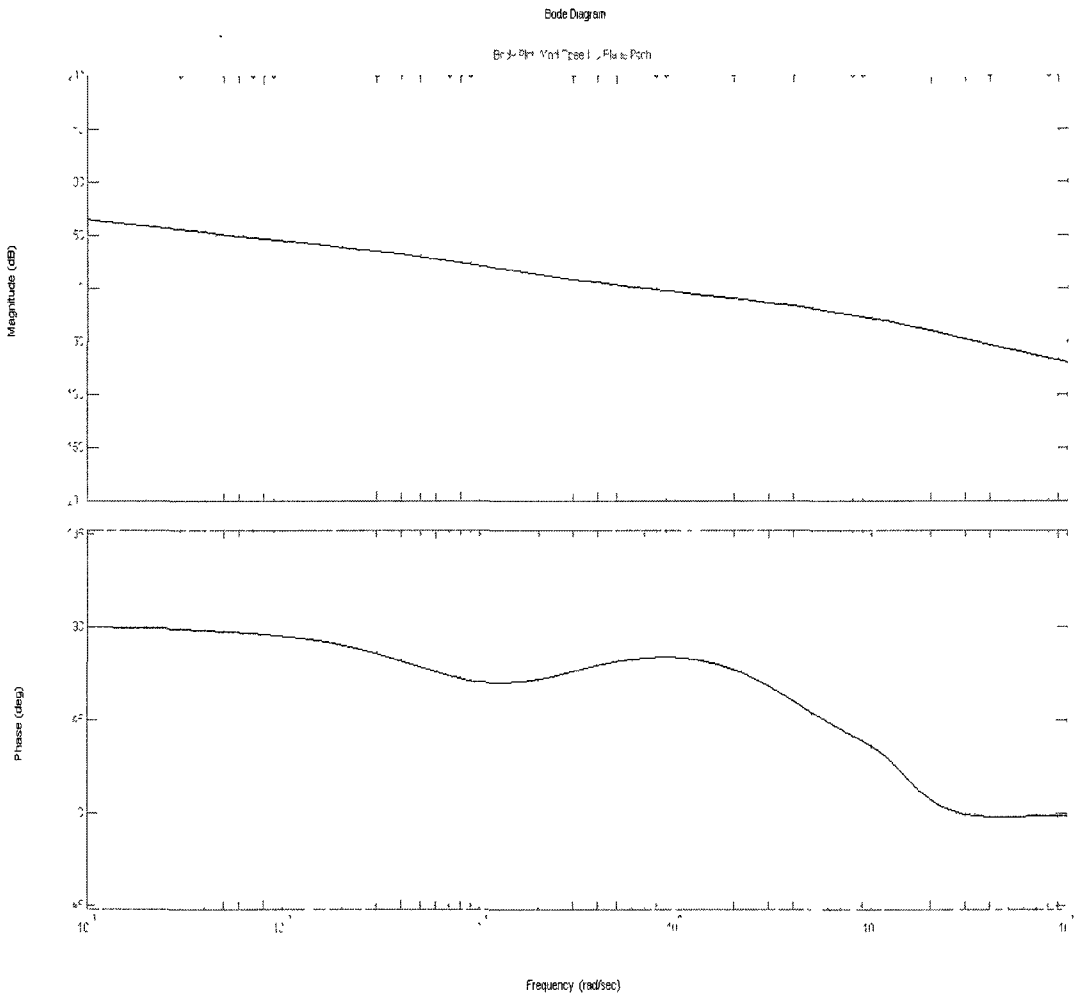

The Bode plots are read in the same manner as described in Chapter 2 to determine the gain and phase margin of the system. As can be seen from the plots the system gain and phase margins are 47 db and 74° respectively. As with the PI Controller, the design criterion is that the gain and phase margins must be large enough to provide headroom for modeling errors and component tolerances. The selected pole locations exceed the design criteria of a minimum gain margin by 41 db and the minimum phase margin of 45^{o} by 29°.

One of the other system criteria is that the blade pitch rate of the system must be kept to a minimum. To check this, the closed loop response to a 1 m/s increase and decrease in the wind speed is reviewed. As can be seen in figures 3.4 and 3.5 the blade pitch response and generator speed stay within the desired characteristics of blade pitch angles that are smaller than 8 deg/s and the generator speed does not increase more than 10% from its steady state value.

Figure 3.4 – Blade Pitch Angle with a step input

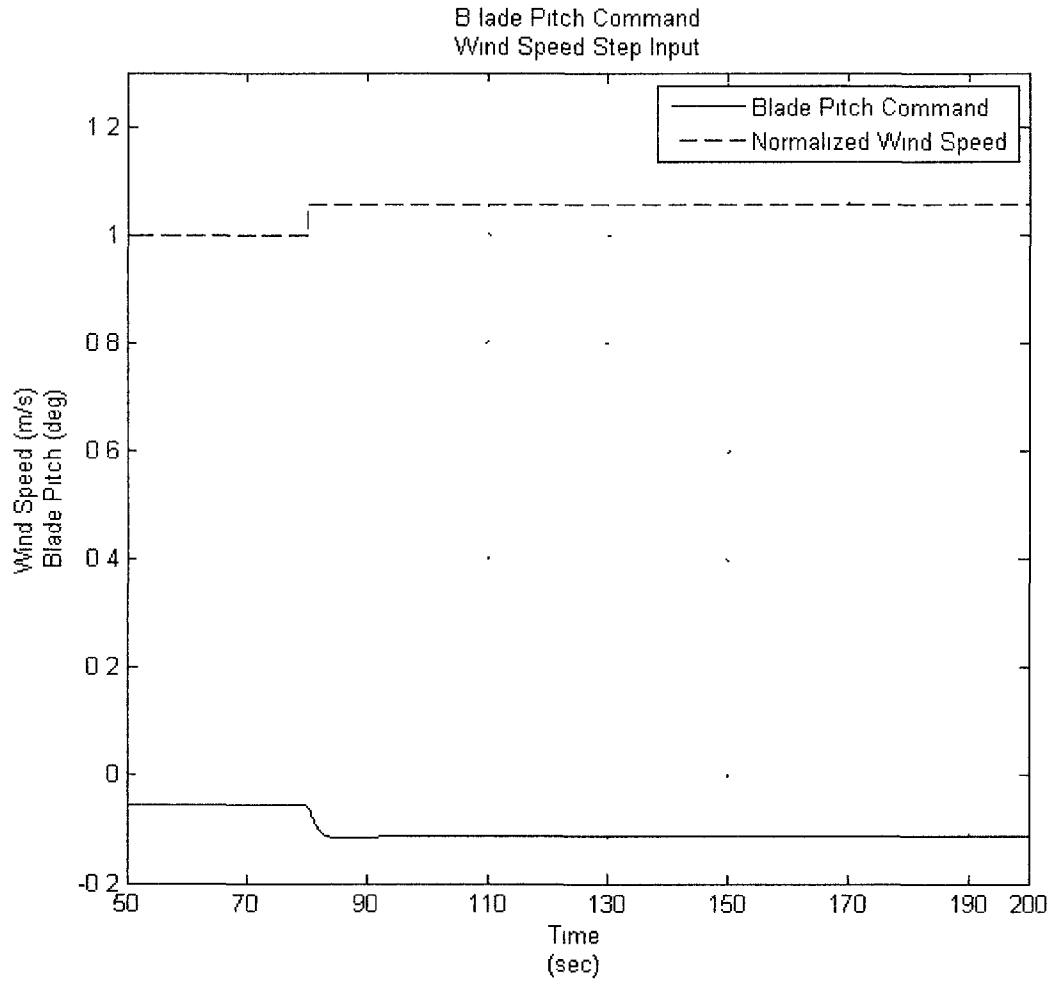

Figure 3.5 – Generator Speed with a step input

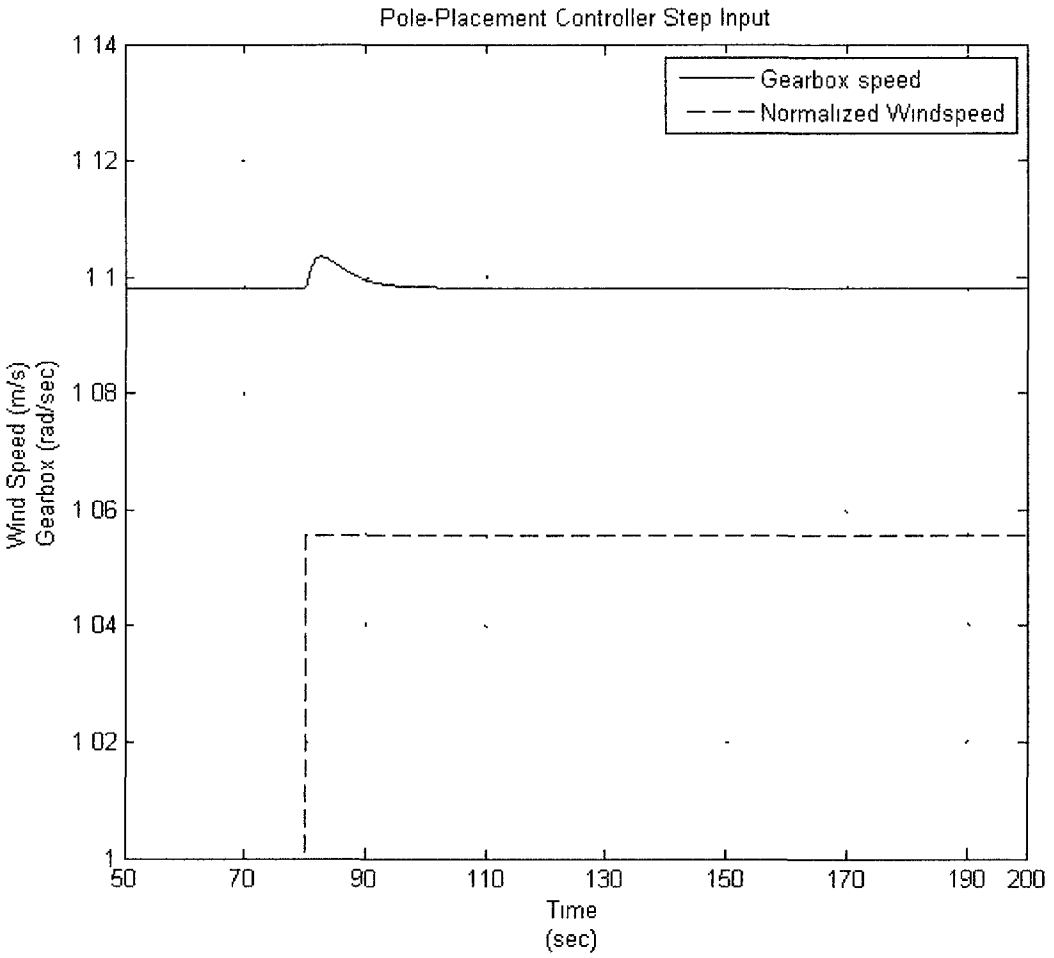

As can be seen from these two graphs the blade pitch responds to the step input by requiring an angular change of 0.1 degrees, and the resulting speed of the generator overshoots the desired operating point by 3% and returns to the desired operating condition in 10 seconds. Because these values are within the range of acceptable system operating parameters, the closed loop response to a step input can be concluded to be a desirable outcome.

Pole Placement Controller Validation

Based on the output of the system and the fact the proper gain and phase margins are maintained, the system can now be checked for its response against a random process input. This is included in the model as a white noise input with a variance of 0.38 m/s^2 and run through a third order filter with a DC gain of 1 and a cutoff frequency of 3 Hz. This filter was selected to represent a random wind process based on the idea that the wind should not see step increases of more the 2 m/s in a time period of 1 second, and that the majority of the power of the wind will be located in the bandwidth between DC and 3 Hz. A review of the Power Spectral Density (PSD) of the wind files used for the final testing of the models in Chapter 5 shows that this is a reasonable approximation for model testing purposes.

The random process of the wind as described above was supplied to the wind turbine system model to determine the amount of lag between the wind torque input and the time at which the system responds to a correction in the generator speed. The results of this random process input are shown below in figure 3.6.

Figure 3.6 – Random Wind Input to Wind Turbine

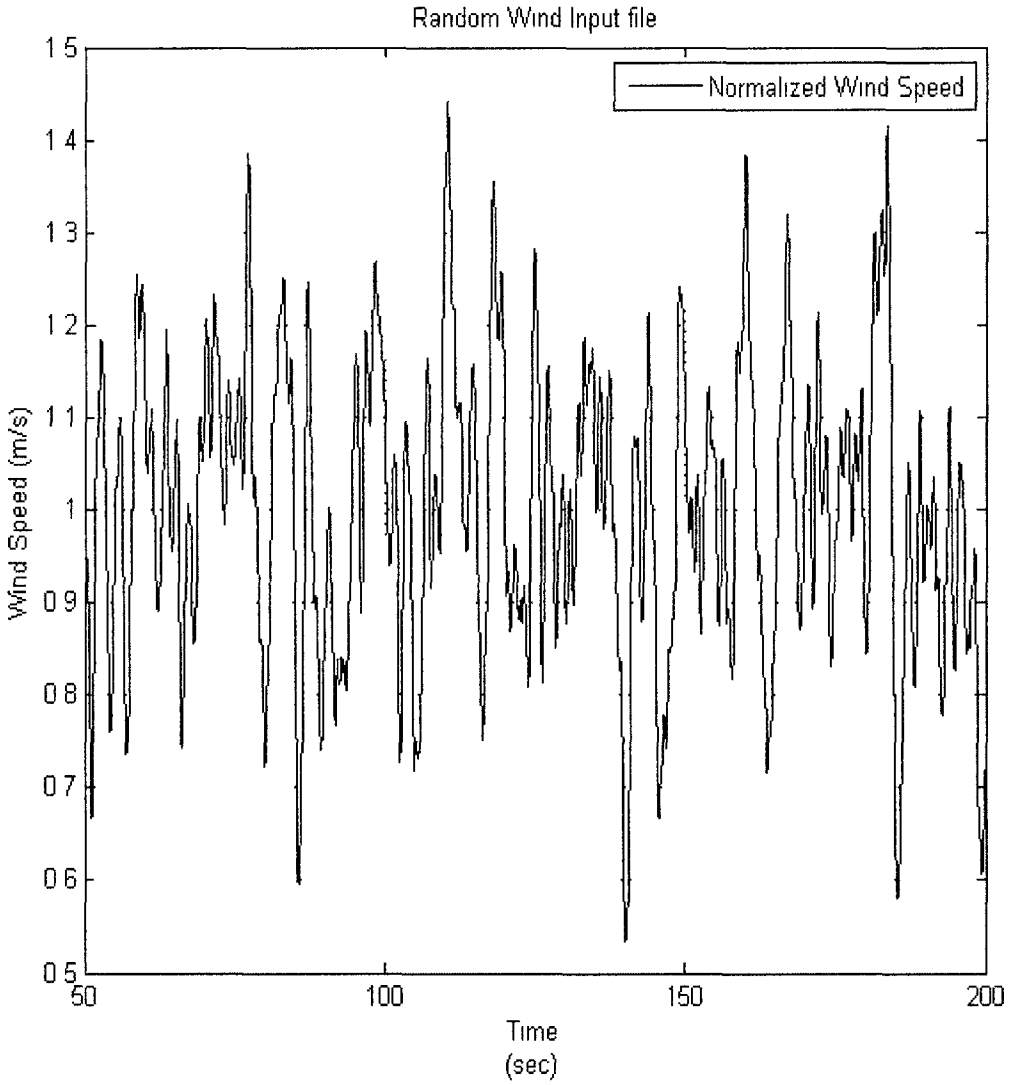

The blades are responding to changes in the input in 2 seconds. This indicates that while the system is successfully mitigating the torque variations on the drive train, it is not providing the optimal result of eliminating the torque variations from reaching the gearbox. Because of the inclusion of the fluid coupler in the drive train, there is the ability to control the fluid coupling coefficient by changing the valve position. By

changing the valve position on the fluid coupler, the system can actually absorb more torque variation from the shaft before it reaches the gearbox. The system can be allowed to accomplish this through the creation of a separate PI controller specifically for the fluid coupler or pole-placement/optimal control can be used so that the blade pitch and fluid coupling do not operate completely separately.

The pole-placement technique allows for the poles to be selected for each of the system inputs. In this case the two system inputs are the blade pitch and the fluid coupling coefficient. By including the fluid coupling as an input state, the $\underline{B_a}$ matrix will change as shown below:

$$\underline{B_a} = \begin{pmatrix} 0 & 0 & 0 & 0 & 0 & 0 & 0 & \frac{J_b}{4.76} \\ 0 & 0 & 0 & \frac{1}{J_f} & 0 & 0 & 0 & 0 \end{pmatrix}^T \tag{3.10}$$

Based on having two inputs to the system, the system controllability must be re-checked as discussed above. The controllability matrix $\underline{C_n}$ is shown to have full rank and the system is controllable.

Because the system is controllable, another pole placement algorithm could be run to find the control gains for each of the two inputs. However, because the system sensitivity to each of the states has not been previously calculated, the pole-placement technique was not used for this particular system. As noted earlier, selecting a large number of poles and testing each of the solutions can become laborious, rather than continue down this path with pole placement. The design focus at this point shifts from

pole-placement to an optimal LQR control design. The design procedure for the optimal control will be discussed in the next chapter.

Chapter 4:

LINEAR QUADRATIC REGULATOR CONTROL

Control System Overview

As noted in earlier chapters of this thesis, one of the other more advanced controllers that can be developed to control the wind turbine system is a Linear Quadratic Regulator or LQR controller. The controller function is much like that of the pole-placement controller developed in Chapter 4. Unlike the pole-placement method, the LQR controller does not allow the designer to select the desired locations for the poles. The LQR controller instead makes use of a cost function to develop the feedback gains for the controller. In the case of the LQR controller, the designer specifies cost penalties for each state instead of selecting desired pole locations. As with the case for the pole-placement controller, the LQR controller does require that every state of the system is available either through measurement or estimation/filtering.

The biggest advantage of using an LQR controller design is that the gain and phase margin issues discussed for the PI controller and pole-placement controller are not dominant issues. The LQR controller, by design, provides for a phase margin of at least 60°. This leads to a robust controller design that will tolerate a number of different component modeling tolerances.

The goals for the LQR controller are the same as for PI controller and the pole-placement controller. The desire is that the controller quickly responds to step changes in the input wind torque with a minimal amount of blade pitch rate and with a minimum amount of controller lag. The generator speed overshoot criteria for the LQR controller is still 10% as in the case of the other two controllers.

Modeling Additions – Control of the Fluid Coupler

Up until this point of the thesis, the only allowable control parameter for the wind turbine has been the blade pitch angle. It was purposely chosen to leave the control of the fluid coupler out of the design of the other controllers for simplicities sake. This additional control parameter will be introduced at this point.

The easiest way to think of a fluid coupler is as a pair of rotating shafts whose sole means of transmitting power between them is a thin layer of high pressure hydraulic fluid. A conceptual view is shown in Figure 4.1.

Figure 4.1 – Basic Fluid Coupler

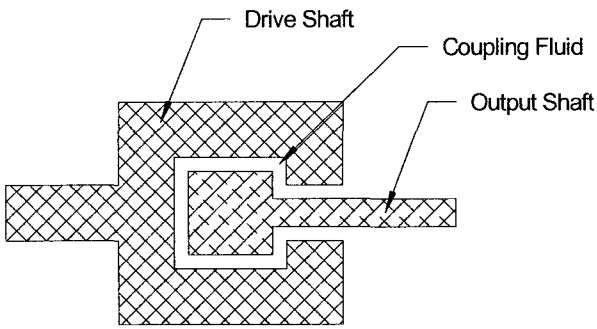

One of the added features of the fluid coupler is that the pressure inside the coupler can be controlled. This means that as the speeds of the shafts start to differ, hydraulic fluid can be bled out or added in to change the coupling coefficient. This leads to a more even flow of energy through the system and allows for a place for extra energy to be absorbed. In addition, as the torque on the front end starts to drop, the coupler can be made to couple the two rotating shafts together more tightly so that the same initial amount of torque is still supplied to the load end of the shaft.

Unfortunately, the ability to control the coupling coefficient is not an instantaneous event. The valve that controls the amount of fluid in the coupler is a solenoid valve and has its own time constant. The electrical time constant for a typical solenoid valve is 0.1 milliseconds. This time constant could be incorporated into the wind turbine system using the following block diagram.

Figure 4.2 – Block Diagram of the Solenoid Valve

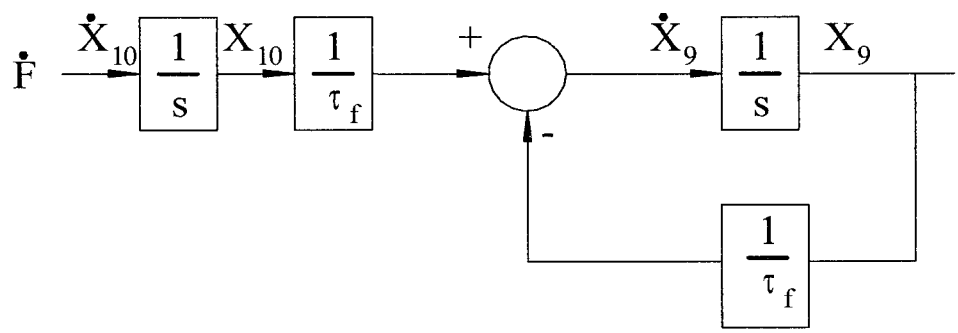

As is the case with the single input controller of earlier chapters, the solenoid valve requires that additional states be included in the A and B matrices so that the system is able to track step inputs in the wind with zero steady state error. Based on the block diagram above, the two additional states to be added into the system are:

$$\dot{X}_9 = -\frac{1}{\tau_f} X_9 + \frac{1}{\tau_f} X_{10} \tag{4.1}$$

$$\dot{X}_{10} = F \tag{4.2}$$

In equations 4.1 and 4.2, $\dot{F}$ represents the rate of input to the solenoid coil, X_{10} is the rate of change of the solenoid coil and X_9 is the command position change of the valve. As is the case with the other elements within this system, all of the solenoid states are linearized around the operating point of 18 m/s. By doing this the state equations in equations in 4.1 and 4.2 change variables to $\Delta\dot{x}$ and Δx instead of the unperturbed states listed above.

While the information on the solenoid valve presented above is correct, it is purposely going to be left out of the design model for simplicity sake. By inspection, it can be seen that the time constant for the solenoid valve is 0.1 ms/4 or 0.025 ms. This

means that the solenoid valve is operating significantly faster than the rest of the mechanical system. This is largely because the solenoid valve is more of an electrical system and responds to inputs more quickly than a mechanical system can. By looking at the pole location of the solenoid valve and the pole locations from the original system, it can be seen that the poles of the solenoid are on average 40x larger than the dominant poles in the system. Refer to equation 3.10 for original pole locations. Because of this observation, the effects of the time delay within the solenoid valve are considered as happening instantaneously, and will be ignored within the wind turbine model.

LQR Controller Set-up

An LQR controller has many of the same requirements as the pole-placement controller developed in chapter 3. One of the requirements for using the LQR controller is that every state of the model must be available. The LQR method assumes that all the measurements are available through sensors, but they could be implemented using any number of different estimator and filter routines. The LQR controller will work with a linearized form of the state equations, so the state space can be implemented as:

$$\underline{\Delta\dot{x}} = \underline{A\Delta x} + \underline{B\Delta u} \tag{4.3}$$

In this equation, as noted above, $\underline{\Delta\dot{x}}, \underline{\Delta x}$, and $\underline{\Delta u}$ are the perturbation variables of the system about the desired operating point. The matrices $\underline{A}$ and $\underline{B}$ are still the state matrix and input matrix respectively, and are in linearized form. In the case of the wind

turbine system that is being analyzed, the A and B matrices are considered to be time-invariant and therefore are constant matrices.

To begin the process of finding the gains needed for implementing the LQR controller, a cost function must be generated. In the case of an LQR controller the cost function is given by (17):

$$J = \frac{1}{2}\int_{t_0}^{\infty}[\underline{x}^T \underline{Q}\underline{x} + \underline{u}^T \underline{R}\underline{u}]\, dt \tag{4.4}$$

In equation 4.4 the matrices Q and R are positive definite matrices that allow for weighting penalties to be placed on each of the individual states. The definition of a positive definite matrix is that the matrix must meet the following form (18):

$$\underline{x}^T \underline{A}\underline{x} > 0 \text{ for any } x \text{ not equal to } 0. \tag{4.5}$$

As seen in equation 4.4, since both Q and R are chosen as positive definite matrices, the functions $\underline{x}^T \underline{Q}\underline{x}$ and $\underline{u}^T \underline{R}\underline{u}$ will always be positive. Because both functions are always positive there exists a controller where the cost function J will be minimized.

From the LQR cost function an optimal control signal u* can be found. The optimal control gains for the system are then given by (17):

$$\underline{u}^*(t) = -\underline{R}^{-1}\underline{B}^T\underline{S} = -\underline{K} \tag{4.6}$$

In equation 4.6 the matrix S is a constant, positive definite square matrix of the form:

$$\underline{S} = \begin{bmatrix} S_{11} & \cdots & S_{1n} \\ \vdots & \ddots & \vdots \\ S_{n1} & \cdots & S_{nn} \end{bmatrix} \tag{4.7}$$

The matrix S is the solution to the following Riccati equation (17):

$$\underline{\dot{S}} = -\underline{SA} - \underline{A}^T\underline{S} - \underline{Q} + \underline{SBR}^{-1}\underline{B}^T\underline{S} = \underline{0} \tag{4.8}$$

As is the case with the pole placement algorithm the optimal control algorithm returns the controller gains of the system in the same form as equation 3.7. In the case of the optimal control algorithm the gain matrix K has been replaced by $\underline{R}^{-1}\underline{S}$. That means the form of the closed loop poles of the system is now given by (17):

$$\underline{\dot{x}} = \left[\underline{A} - \underline{BR^{-1}S}\right]\underline{x} \tag{4.9}$$

The eigenvalues of the closed-loop system$\left[\underline{A} - \underline{BR^{-1}S}\right]$ are all in the left half s-plane and are therefore stable (17). It can then further be stated that the minimum cost function is now given by (17):

$$\underline{J} = \frac{1}{2}\underline{x}^T\underline{Sx} \tag{4.10}$$

It should be noted that in all of the equations listed above the time function has been removed for equation simplicity and is actually implicit in the variables x and u. This section is also not intended to be a full review of generating the optimal control gains of a system. For a more thorough review of this process, it is suggested that one review *Optimal Control* by Frank Lewis listed in the reference section of this thesis.

It can be seen from equations 4.7 and 4.8 that the solution to the Riccatti equation can be found by hand. To accomplish this, all of the matrix math must be done to create n independent equations. From these equations each of the elements S_{ij} can be found, and the resulting optimal closed loop gains, K, can be found. Because of the

size of matrices involved, doing the calculations by hand can easily result in unintended errors, and it does not allow for iterations upon the penalty matrices to be run quickly. At this point it is best to turn solving for the gain matrices over to a computer program. In this case MATLAB™ and its "lqr" function are used to solve for the optimal gain coefficients, and allow for the iterations necessary to design a controller that meets the design performance criteria set forth earlier in this thesis.

Up until this point, the roles and forms of the Q and R matrices have been left undefined. Both of the matrices are square matrices with all of the off-diagonal terms set to zero. There are a couple of reasons for doing this. The first one is that by setting the off-diagonal terms to zero and using only positive penalty values on the diagonal terms, a positive definite matrix is guaranteed. The second reason is that the controller is not designed to take feedback from coupled states within the model. That means that it is not applying gains or penalties to the state combinations such as that of X_1X_2. The purpose of the Q matrix is to apply penalties on each of the states of the system. As can be seen by looking at equation 4.4 and the definition of the Q matrix, the diagonal values of the Q matrix apply a weighting value to the squares of each of the states in the model. That means that a penalty can be applied to each state as it moves further away from its desired set point.

The R matrix applies penalties to the control input. In the case of a single input system R will be a scalar quantity. However, when the system has multiple inputs it will be a square matrix with the same number of rows and columns as there are inputs. In the case of the model that is being reviewed in this thesis, the R matrix is a 2x2 matrix as

there are two inputs that can be controlled: the pitch angle of the blade and the coupling coefficient of the fluid coupler. As noted above, there are only penalties applied to the r_{11} and r_{22} terms and the off-diagonal values are set to zero.

The addition of the R matrix, or penalties on control effort, into the calculation of the system feedback gains is one of the major differences between the optimal control technique and pole-placement. The pole-placement algorithm requires that new pole positions be found, but it does not guarantee any limits on the control inputs. The only way to find these limits is to test the model through a number of different iterations. By using optimal control, and specifically the penalty matrix R, the designer can adjust expectations on how large the control input can be during the initial system set-up. This is actually a very important concept to include in the design criteria for a wind turbine. The control system commands cannot be allowed to vary wildly as these would put additional stresses on the motors to change the blade pitch angle and the solenoid valve. It may not be intuitive to put a limit on the solenoid valve motion, but one of the situations that needs to be avoided is a water-hammer effect. A water hammer is caused by abruptly changing values of the fluid pressure within the coupler, and can result in significant damage to the system if it occurs repeatedly.

System LQR Controller Development

The remainder of this chapter is devoted to the development of a two input, LQR controller to regulate the generator speed. As noted, the two input variables are the blade pitch angle and the solenoid valve position. The addition of this new control

variable changes the B matrix from a 1 x 8 matrix to a 2 x 8 matrix. This results in the gain matrix $\underline{K} = \underline{R}^{-1}\underline{S}$ having two rows of system gains for each of the two inputs. In addition to this the system matrix $\underline{A}$ must also be augmented to include the additional state from the solenoid valve control. The states of the system are as noted in 4.11 and the new $\underline{A}$ and $\underline{B}$ matrices are as shown in equations 4.12 and 4.13

$$\underline{\dot{\Delta x}} = \begin{pmatrix} \Delta\dot{e} \\ \Delta\ddot{\theta}_4 \\ \Delta(\dot{\theta}_3 - \dot{\theta}_4) \\ \Delta\ddot{\theta}_3 \\ \Delta(\dot{\theta}_2 - \dot{\theta}_3) \\ \Delta\ddot{\theta}_2 \\ \Delta(\dot{\theta}_1 - \dot{\theta}_2) \\ \Delta\ddot{\theta}_1 \end{pmatrix}, \quad \underline{\Delta x} = \begin{pmatrix} \Delta e \\ \Delta\dot{\theta}_4 \\ \Delta(\theta_3 - \theta_4) \\ \Delta\dot{\theta}_3 \\ \Delta(\theta_2 - \theta_3) \\ \Delta\dot{\theta}_2 \\ \Delta(\theta_1 - \theta_2) \\ \Delta\dot{\theta}_1 \end{pmatrix} \tag{4.11}$$

$$\underline{A} = \begin{pmatrix} 0 & -1 & 0 & 0 & 0 & 0 & 0 & 0 \\ 0 & -\frac{B_g + D_f}{J_g} & \frac{N^2 * K_f}{J_g} & \frac{N^2 * D_f}{J_g} & 0 & 0 & 0 & 0 \\ 0 & -1 & 0 & 1 & 0 & 0 & 0 & 0 \\ 0 & \frac{D_f}{J_f} & -\frac{K_f}{J_f} & -\frac{D_r + D_f + B_f}{J_f} & \frac{K_r}{J_f} & \frac{D_r}{J_f} & 0 & 0 \\ 0 & 0 & 0 & -1 & 0 & 1 & 0 & 0 \\ 0 & 0 & 0 & \frac{D_r}{J_r} & -\frac{K_r}{J_r} & -\frac{D_r + D_b + B_r}{J_r} & \frac{K_b}{J_r} & \frac{D_b}{J_r} \\ 0 & 0 & 0 & 0 & 0 & -1 & 0 & 1 \\ 0 & 0 & 0 & 0 & 0 & \frac{D_b}{J_b} & -\frac{K_b}{J_b} & -\frac{B_b + D_b}{J_r} \end{pmatrix} \tag{4.12}$$

$$\underline{B} = \begin{pmatrix} 0 & 0 & 0 & 0 & 0 & 0 & 0 & \frac{J_b}{4.76} \\ 0 & 0 & 0 & \frac{1}{J_f} & 0 & 0 & 0 & 0 \end{pmatrix}^T \tag{4.13}$$

Based on the original design criteria, the Ricatti equation shown in equation 4.8 is solved to find the gain matrix $\underline{K}$. As noted above the $\underline{Q}$ and $\underline{R}$ matrices takes on the form:

$$\underline{Q} = \begin{pmatrix} q_{11} & \cdots & 0 \\ \vdots & \ddots & \vdots \\ 0 & \cdots & q_{88} \end{pmatrix}, \ \underline{R} = \begin{pmatrix} r_{11} & 0 \\ 0 & r_{22} \end{pmatrix} \tag{4.14}$$

In these matrices the q_{nn} and r_{nn} are the penalties applied to each of the states of the system. The specific meaning of each of the penalties is as noted in Table 4.1.

Table 4.1 – LQR Penalty State Assignments

Penalty	Associated State	Description
$q_{1,1}$	Δe	Penalty on the integrated gearbox speed error
$q_{2,2}$	$\Delta\dot{\theta}_4$	Penalty on the gearbox speed error
$q_{3,3}$	$\Delta(\theta_3 - \theta_4)$	Penalty on the difference between the output fluid coupler and the gearbox shaft positions
$q_{4,4}$	$\Delta\dot{\theta}_3$	Penalty on the fluid coupler speed error
$q_{5,5}$	$\Delta(\theta_2 - \theta_3)$	Penalty on the difference between the rotor position and the input fluid coupler position
$q_{6,6}$	$\Delta\dot{\theta}_2$	Penalty on the rotor speed error
$q_{7,7}$	$\Delta(\theta_1 - \theta_2)$	Penalty on the difference between blade and rotor positions
$q_{8,8}$	$\Delta\dot{\theta}_1$	Penalty on the blade speed error
$r_{1,1}$	ΔB	Penalty on the rate of change on the blade angle
$r_{2,2}$	ΔF	Penalty on the rate of change of the solenoid valve

Each of the penalties shown in the table 4.1 is assigned a weight through an iterative process. The iterative process for assigning the penalty weights to each of the states is started by making each of the states count equally in the cost penalty function. This can be determined by running the system in an open loop configuration and measuring the squared values of each of the states and then taking the inverse,

meaning taking the weighted time average of each state, $< \frac{1}{x_i^2} >$. This can only be taken as a starting point for the system, as closing the loop with the resulting gain values does not often produce satisfactory results. From the initial iteration of the design set points the designer can get a feel for how each of the penalties applied to the system affects the output and subsequently the eigenvalues of the system. By iterating through these values, several different aspects can be learned about the system penalties. The first observation is that the penalty on the integrated error of the gearbox speed is critical (q_{11}). If this value is set too low, the wind turbine will never come up to the desired speed, and if set too large the system asks for very large changes to the input parameters. The next largest contributing factor is the actual velocity of the gearbox. This primarily affects the system overshoot and ringing frequency. The absolute position penalties are found to be approximately equal across the system and mainly affect how quickly the overshoot and oscillations are damped out of the system.

Through the iterative process the desired penalties and gains for the wind turbine plant are set as follows:

Table 4.2 – Parameter Values for Q and R matrices

Penalties		Feedback Gains				Eigenvalues
$q_{1,1}$	150	$k_{1,1}$	-3.162	$k_{2,1}$	-0.9408	-2.14E+07
$q_{2,2}$	100	$k_{1,2}$	1.409	$k_{2,2}$	2.946	-6129
$q_{3,3}$	1000	$k_{1,3}$	0.446	$k_{2,3}$	0.133	-7.644+11.69j
$q_{4,4}$	900	$k_{1,4}$	0.002	$k_{2,4}$	2.232	-7.644-11.69j
$q_{5,5}$	1000	$k_{1,5}$	16.921	$k_{2,5}$	4.564	-23.739
$q_{6,6}$	5000	$k_{1,6}$	13.812	$k_{2,6}$	0.676	-2.0548
$q_{7,7}$	800	$k_{1,7}$	8.489	$k_{2,7}$	-0.045	-0.1466
$q_{8,8}$	500	$k_{1,8}$	5.773	$k_{2,8}$	0.000	-1.06E-05
$r_{1,1}$	15					
$r_{2,2}$	0.000025					

There is one item of particular interest to note in Table 4.2. The eigenvalue for one of the poles is located at -1.06E-5. This is a very slow pole, but it is not the dominant pole of the system. This is because the pole at -1.06E-5 is associated with the total inertia of the system, which cannot change quickly because of its physical size. A considerable amount of design effort was centered on trying to move this pole to a faster location. Despite this effort, it was found that attempting to move this pole even a minimal amount from its starting location required extreme effort upon the part of the controller, and resulted in blade pitch saturation and rate limit errors. A similar result was found during the pole placement design in chapter 3. As a result this one pole remained very close to its original open loop location.

Another of the results of that can be seen from table 4.2 is that the penalty on the input to the fluid coupler is significantly smaller than the penalty on the wind power

input. This factor is a result of the small value of the inertia of the rotating fluid in comparison with the mass of the blades and rotor. It should also be noted that the input to the fluid coupler contains an offset of approximately 0.5, representing that it is normally in the half way open position. This offset can be changed by adjusting the penalty on r_{22}. Care must be taken when adjusting this value in the model as the computer simulation will allow the fluid coupler input to take on gains of greater than 100% when saturation is not included in the model.

The data flow from the dual input LQR controller is similar to that of the pole-placement controller. The major difference between these two controllers is that the LQR controller has two sets of gains associated with each one of the states, whereas the single input pole-placement controller has only one gain per state. The gains for the LQR controller are implemented as shown below in Figure 4.3. Because of all the additional gains in the system, the signal diagram does become significantly more difficult to follow, but can be represented in block form as shown in Figure 4.3.

Figure 4.3 – Multi-Input LQR Controller Implementation

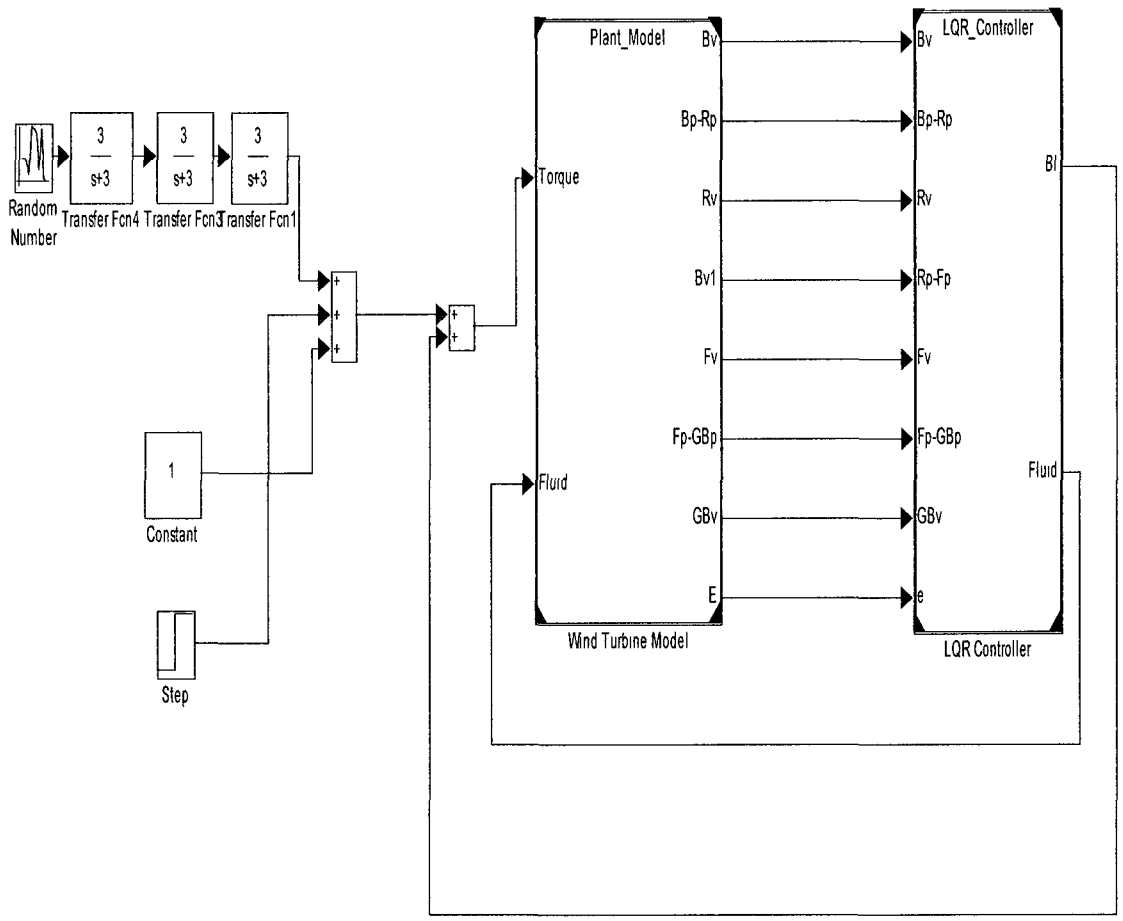

Multi-Input LQR Controller Validation

In order for the system gains of the LQR controller to be validated, a number of different inputs were put into the wind turbine system see how the controller would react to them. As with the cases of the previous controllers, this controller was given a step input. The step input used is the equivalent to a 1 m/s change in the input wind velocity. The resulting gearbox speed as a result of the step input is shown in figure 4.4.

Figure 4.4 – Step Input Gearbox Speed Response

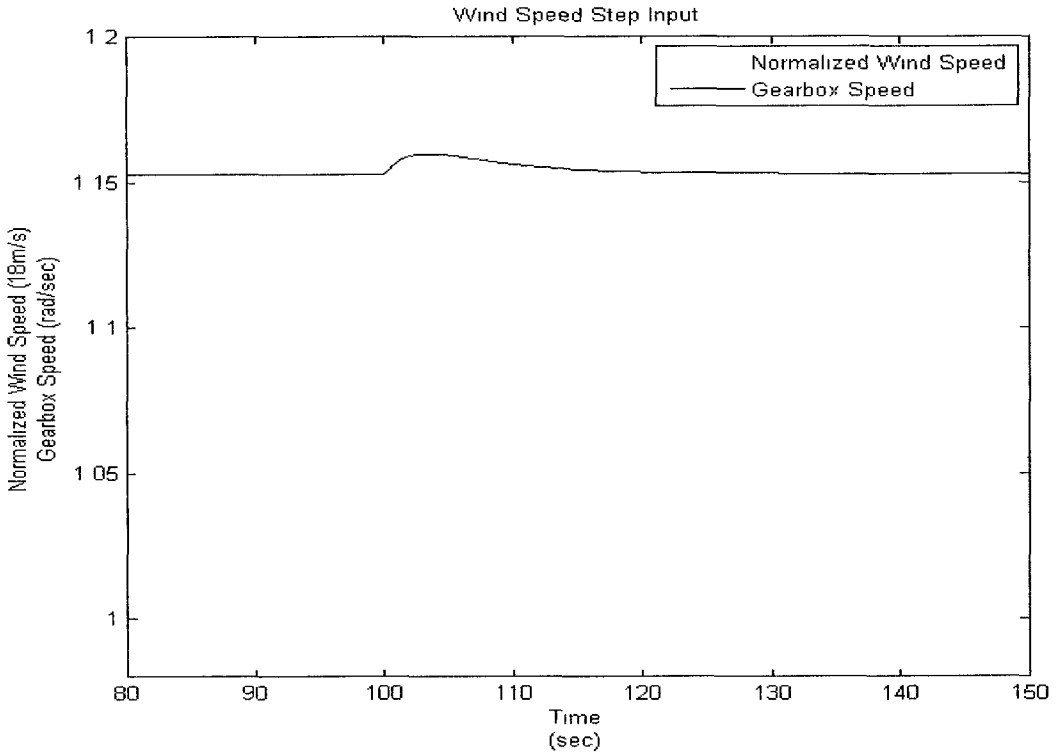

In comparison with the other controllers presented in this thesis the two input LQR controller has a slightly smoother transition and less variation in gearbox speed than the other controllers. This initial result indicates that the LQR controller should result in better overall system regulation of variable inputs in wind speed.

As noted earlier in this chapter, one of the main advantages of a single input LQR controller is that it will guarantee a minimum of 60° of phase margin. The one item that does need to be reviewed is the frequency at which the gain of the system falls off. It is important that this stays above a few hertz so that the majority of the power generated by the wind can be used. A Bode plot of the closed loop LQR controller is shown in figure 4.5.

Figure 4.5 – Bode Plot of the Closed Loop LQR controller

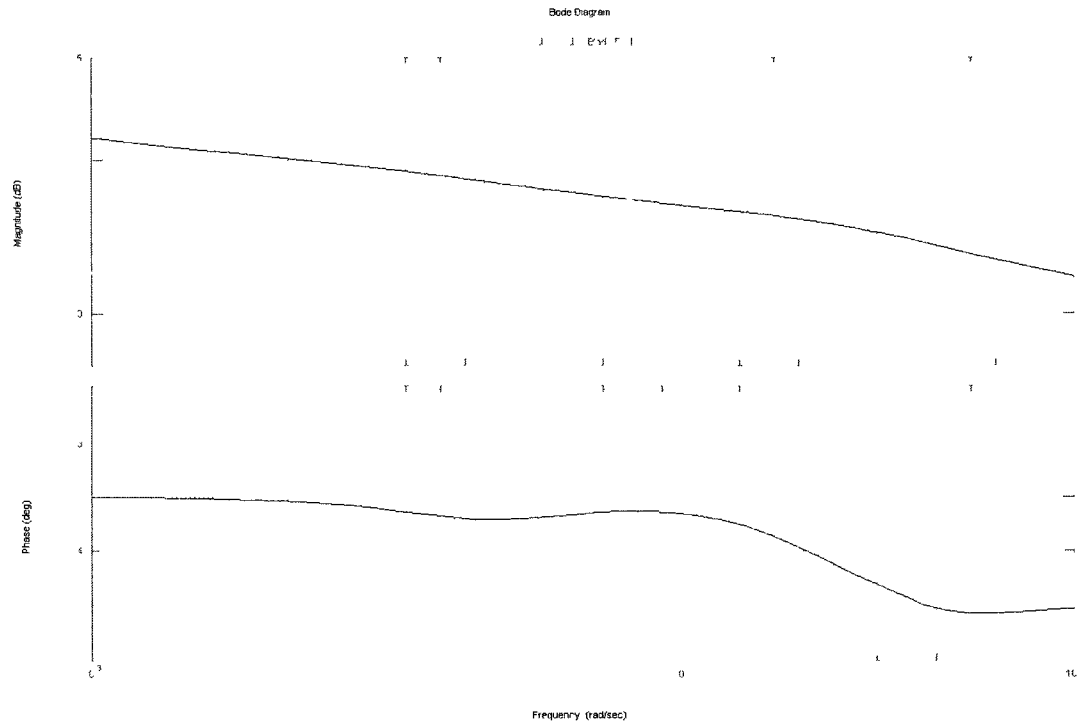

As can be seen from the Bode plot the 0 db crossing is at a frequency of 1.9 Hertz. This is high enough to allow for control of the majority of the wind power coming into the system.

As mentioned previously, one of the major design constraints of any of the controllers developed is that the blade pitch angles cannot make rapid changes. In addition to this limitation, one of the other items that needs to be mitigated is the changes in the solenoid value position. As is the case with the change in blade pitch angle, the solenoid valve needs to have small smooth changes in position. If this were not the case, large pressure variations could be developed in the fluid coupler that could eventually cause damage to the system, either through fluid hammering or excitation of

one of the resonant frequencies within the system itself. As was the case for the pole-placement controller the LQR controller was subjected to both an increase and decrease in wind speed of 1 m/s. The resulting control signals generated for both the blade pitch and the solenoid valve are as shown in Figure 4.6.

Figure 4.6 – Blade Pitch and Solenoid Valve Position Control Signals

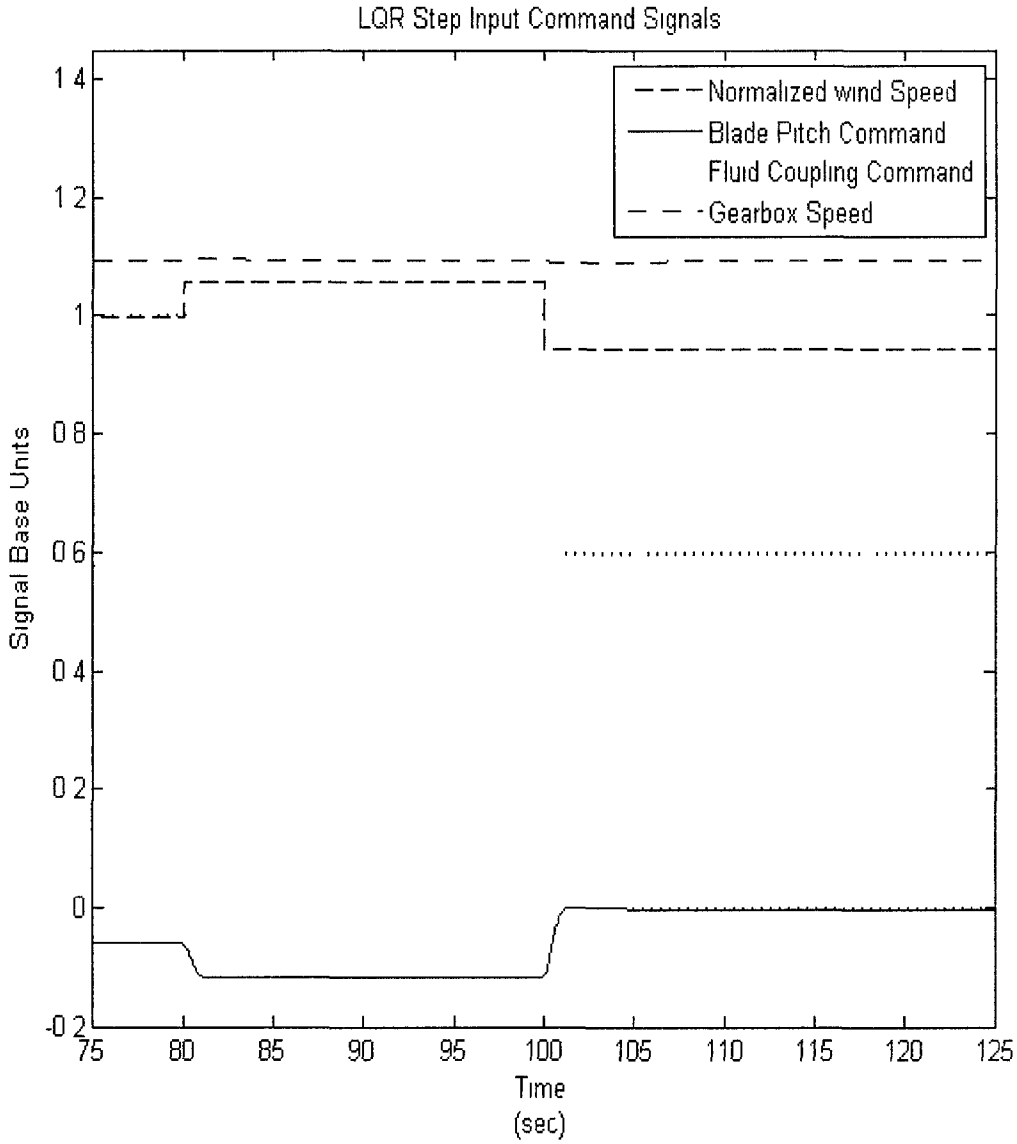

As can be seen from the graph above, both the blade pitch and solenoid valve control signals react to the step input in 2 seconds, and the gearbox speed is controlled within 7 seconds. By doing a quick comparison with the results shown in figure 3.4, it can be seen that the additional control on the solenoid valve reduces the response required by the blade angle. This result should be expected as the addition of the solenoid valve starts to decouple gearbox velocity from the input wind speed by adding or removing additional damping from the system.

CHAPTER 5:

SIMULATION RESULTS AND ANALYSIS

Simulation Overview

In the preceding three chapters the design procedure for three different types of controllers was discussed. Those chapters went into detail on how each of the feedback gain parameters was set, and what the tradeoffs were for making changes to those gains. For the most part there was little or no discussion on how each of the controllers would respond to situations that would normally be seen in field operation. The controllers were optimized to respond to small step changes in the input wind speed. In this chapter the controllers will be subjected to simulations that more appropriately mimic actual wind speed changes that occur while the wind turbine is in operation.

For simulated operation in the field, the following assumptions are made to allow for ease of modeling and the control of the system.

1. All of the wind turbine blades are moved simultaneously, and are modeled as a single inertia and flex.
2. The wind speed is uniform across each of the blades
3. The average wind speed shall be 18 m/s (in the middle of operation of Region 3).

4. There is no slipping within the gearbox, i.e. the speed difference between the LSS and HSS is determined strictly by the gear ratio.
5. The back torque applied to the generator is a constant, and does not vary with speed.
6. The fluid properties of the fluid coupler are constant over time, i.e. the spring and damping coefficients are assumed to not change with heat and/or wear.

These assumptions are used as the baseline for comparing the operation of the three different derived control systems discussed in this thesis. For a comparison of each of the controllers, the models are driven by a random wind speed file that approximates the normal changes in wind speed as would be seen by the wind turbine in the field. Simulations based on these controllers are run in Simulink® and include the following model descriptions:

- Simulation of the PI controller with no fluid coupler control
- Simulation of the Pole-Placement Controller with no fluid coupler control
- Simulation of the LQR Controller with both blade pitch and fluid coupler control.

Each of the simulations is run for a total of 250 seconds and has a sampling time of 0.0005 seconds. The small sampling time is a result of the dynamics of the fluid coupler, which corresponds to the extremely large pole location noted in chapter 3. The simulation starts with the blades and all other system elements at a zero value initial

condition. When the simulation is initiated, the blades are immediately driven with an input equivalent step input that causes the wind speed to jump from 0 m/s to 18 m/s. Because the system has been linearized to operate at 18 m/s steady state, this spike input is not within the operating parameters for which the system has been modeled. For the purpose of comparing each of the systems, this initial transient response will be ignored and only the steady state variations will be analyzed. This is because none of these controllers is really designed to handle a step increase of this size and the system demands very large outputs on the blades, and also the fluid coupler in the case of the LQR controller. The step response reaches a steady state for each of the models within 50 seconds. For that reason all measurements and comparisons will begin from that point.

Each of the systems will be compared based on the five critical system parameters listed below in table 5.1.

Table 5.1 – Critical System Parameters and Descriptions

System Parameter	Description
Max Pitch Rate, $\lvert\dot{\beta}\rvert$	Maximum pitch rate of the blades is analyzed and compared to the maximum allowable rate of 8°/sec
RMS Pitch Rate, $\dot{\beta}$	The rate of pitch change in the blades is analyzed to how fast the blade angles are changing in the simulations
STD $\theta_1 - \theta_2$ (Blade Flex)	The standard deviation of the blade flex is analyzed as a measure of fatigue on the blade. The blade flex causes most of the torque variations that propagate down the drive train and that can pass through to the gearbox.
STD $\theta_2 - \theta_3$ (LSS Flex)	The standard deviation of the LSS flex is analyzed as a measure of fatigue on the LSS. As the low speed shaft flexes the torque is passed from the LSS to the fluid coupler
RMS Gearbox Acceleration, $\ddot{\theta}_4$	The Gearbox acceleration is measured to see how fast the speed of the gearbox is changing. This translates into how much the torque is changing on the generator
RMS Gearbox Jerk, $\dddot{\theta}_4$	The change in the acceleration of the gearbox is measured to show the propagation of the rate of torque variations in the gearbox
RMS Gearbox Speed Error, $\Delta\dot{\theta}_4$	The speed error is a measure of how well the controller is controlling the gearbox, and therefore the generator speed.

Wind Input Files

There are a number of different programs available that allow for the modeling of changes in wind speed over what would be the entire plane of the blades. In the case

of the systems and control algorithms developed in this thesis, these are slightly more complicated than are needed to provide testing results. Programs such as Turbsim have been used previously to analyze the linear models developed for this thesis (9). By using the statistics generated by Turbsim and filters created in Simulink, similar wind speed inputs and variations can be modeled.

The input to the filter is the random number generator within the Simulink Source codes. One of the features of the Simulink® Random Number Generator is that by setting the seed to a specified value it allows a consistent set of random numbers to be generated. This allows all of the different models generated to be tested using the same input parameters without the need to create a separate wind speed generating file. It is important to note that the variance within the random number generator must be divided by the step time used in the simulation files to result in the variance that is desired. In the case of this thesis the step size used was 0.0005 seconds. The reason for this small step size can be seen by reviewing the open and closed loop eigenvalues of this system. In particular, the eigenvalue at -6129 needs to be accounted for or it can result in convergence errors because of the speed associated with this pole.

The input filter for the random number generator is a cascade of three single order filters each with a DC gain of 1. Each of the filters is of the form:

$$\frac{\lambda}{s+\lambda} \tag{5.1}$$

By selection of λ the bandwidth of the filter can be chosen to meet the desired requirements. The λ value in the numerator and denominator need to match to allow for a DC gain of 1. In the case of the models and control systems developed in the earlier chapters, the -3db frequencies will be set to 3 Hz and 2 Hz, and will be used to drive each of the derived models. The 2 and 3 Hz cutoff frequencies are chosen to reflect the standards that are used in the Turbsim to generate wind files that are used to test the FAST model developed by NREL.

Figure 5.1 – Wind speed Input model

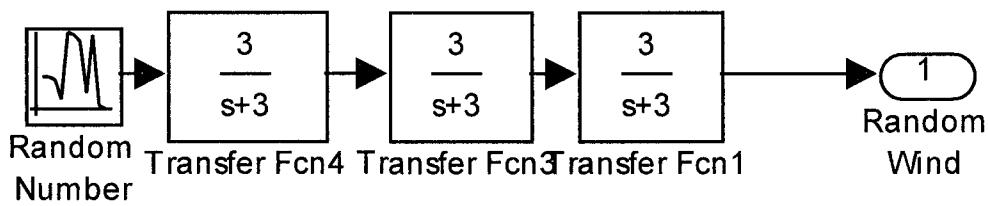

Simulation Results and Discussion

In order to perform a representative analysis of the different systems it is important to do a comparison with a baseline system. Because there is not a fully developed model to which the results of the fluid coupler drive train can be compared, I use the wind turbine model without the fluid coupler as the baseline model. This will provide some insight into how the system may behave in the field as the baseline model has already been shown to be a simplified model of the actual wind turbine system (9).

The analysis of the system/controller design begins by comparing the wind turbine model without the fluid coupler to the PI controller developed in chapter 2. I then subsequently discuss the results of the Pole-Placement Controller developed in chapter 3 and the Multi-input LQR Controller developed in chapter 4. In each case I examine the system parameters defined in Table 5.1. Each model is run with two different random wind input files as described above. The two different inputs are as defined below in Table 5.2

Table 5.2 – Wind Input File Statistics

Wind Speed Statistics	2 Hz File	3 Hz File
Mean	18 m/s	18 m/s
RMS	18.02 m/s	18.08 m/s
Standard Deviation	0.543 m/S	0.389 m/s
-3db Frequency	2 Hz	3 Hz
Min/Max	16.42, 19.43	16.86, 19.08 m/s

One of the advantages to using the random wind speed input file developed in this thesis is that the selection of the starting seed in the SIMLINK™ dialog box allows for a one to one file comparison. The seed number allows the program to create the same pattern of random numbers across multiple files without the need to export and input the values into a workspace array. In addition to this having the same input file allows for easier tuning of the control system parameters because using the same input file allows you to show run to run parameter variation.

The effectiveness of the each of the control systems is measured against a wind turbine model without the fluid coupler present. Each of the control systems is tested with two different wind files driving the blade torque. To begin, the two PI controllers are compared for the statistics noted in table 5.1.

Table 5.3 – PI Controller Statistic Comparison

	Turbine Only		PI Controller	
Parameter	2 Hz	3 Hz	2 Hz	3 Hz
Max Pitch Rate, (deg/sec)	0.4764	0.2725	0.4711	0.2768
RMS Pitch Rate, (deg/sec)	0.2079	0.138	0.1937	0.1119
STD Blade Flex (rad)	0.0013	8.93E-04	0.0012	8.38E-04
STD LSS Flex (rad)	2.15E-04	1.37E-04	1.72E-04	1.11E-04
RMS Gearbox Acc (rad/sec^2)	0.0168	0.0124	0.0163	0.0123
RMS Gearbox Jerk (rad/sec^3)	0.0226	0.0262	0.0224	0.024
RMS Gearbox Speed Error (rad/sec)	0.0525	0.0319	0.0393	0.0237

Table 5.3 was turned into a bar graph to allow for visualization of the data and easy comparison. In each case all of the parameters have been normalized to the Turbine Only data for the 2 Hz input file.

Figure 5.2 – Normalized PI Controller Statistics

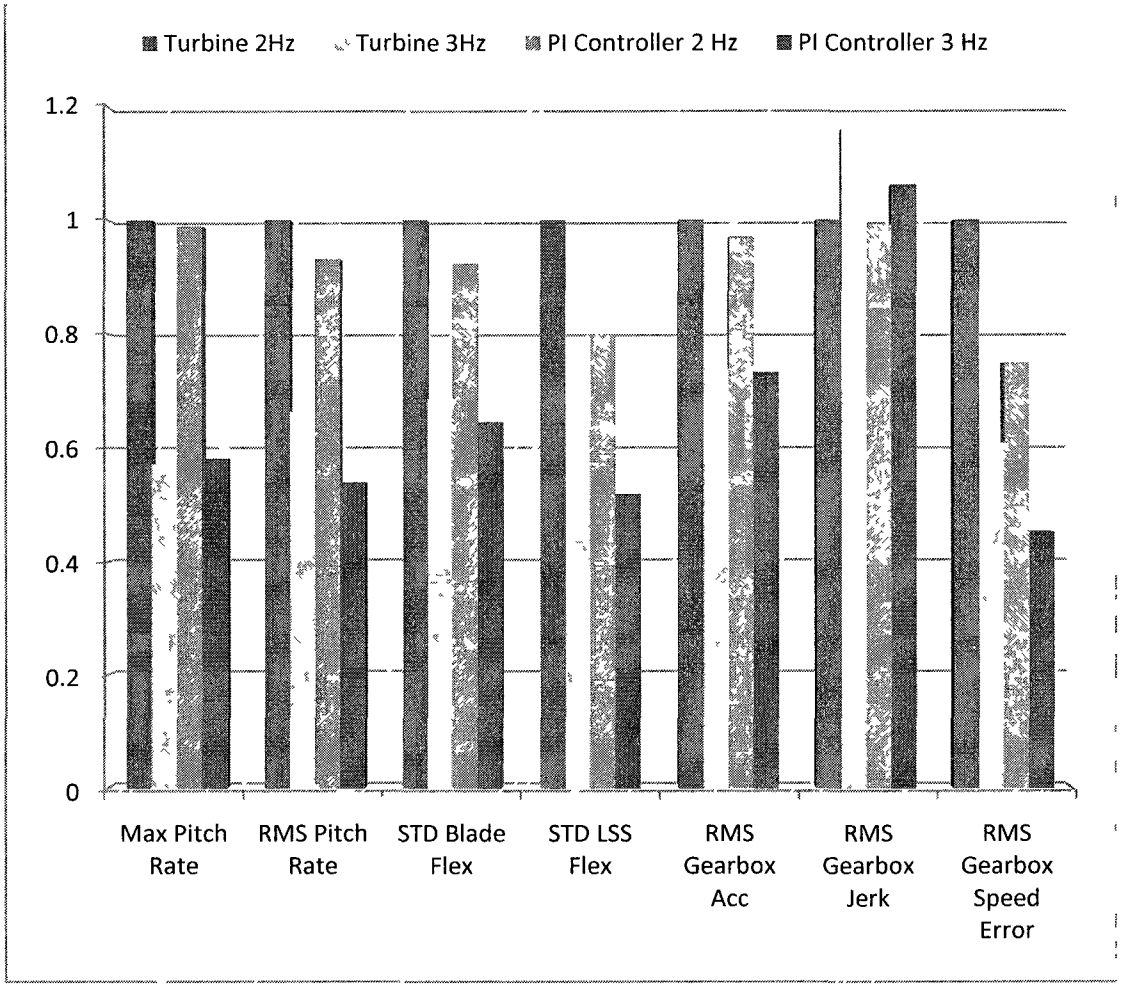

There are a number of interesting observations that can be seen from looking at the data above. The first item of interest is the gearbox jerk value between the 2 and 3 Hz input files. It can be seen from the chart above that the jerk is actually higher for the 3 Hz file even though the wind speed input standard deviation is smaller. The reason for this lies in the Bode plot for the system. Because the -3 db frequency has been moved

to a higher value, the input filter allows for more high frequency power to pass through into the system. Because the input filter allows more of the higher frequency components to pass to the system, it does rely on the system to attenuate the higher frequency components. Unfortunately, this attenuation comes in the form of losses and additional strains on the individual components within the wind turbine itself.

Another of the items that can be seen by looking at the bar chart is that the PI Controller with the fluid coupler is actually running with a tighter control loop. Because of that difference, the Maximum Blade Pitch Rate and the RMS Blade Pitch Rates are slightly higher than for the turbine only. The result of having the tighter loop is that the other parameters of interest are significantly smaller for the turbine that includes the fluid coupler. One of the biggest improvements is that the gearbox speed error for the PI Controller with the fluid coupler is 30% smaller than that of the turbine without the fluid coupler. In addition, there is also about a 10% reduction in the gearbox acceleration. The effect of this reduction in the acceleration is that the torque variation seen by the generator is also reduced.

One of the items that is not revealed in these statistics is the maximum speed of the generator. The reason that this is left out of the statistics is that it can be inferred from all of the other data measurements without explicitly calculating it. It stands from common knowledge that if the RMS value of the error is smaller (difference between the reading and a fixed value), then the difference between the gearbox speed and the

desired speed is also smaller. Therefore, with a fixed gear ratio, as proposed in this study, the generator speed must linearly follow the same trajectory as the gearbox speed.

As the controllers for the wind turbine become more advanced and feedback data is provided from additional states, the pitch commands required on the blades become larger. This is an expected outcome of the control philosophy that was selected. In this study the goal of the controller was to minimize the stresses on the gearbox and keep the generator running at a constant speed. As a result, the control effort to make this happen must be applied to either the blades or the fluid coupler. In the case of the Pole-Placement Controller developed in chapter 3, I am allowing the blade pitch angle to be changed in efforts to control the gearbox speed. The results from running the Pole-Placement Controller are shown in Table 5.4 below, and are compared, as was previously done, in bar chart format in Figure 5.3

Table 5.4 – PI Controller Turbine Only vs Pole-Placement Controller with Fluid Coupler

	Turbine Only		Pole-Placement	
Parameter	2 Hz	3 Hz	2 Hz	3 Hz
Max Pitch Rate, (deg/sec)	0.4764	0.2725	0.7213	0.4637
RMS Pitch Rate, (deg/sec)	0.2079	0.138	0.3238	0.1932
STD Blade Flex (rad)	0.0013	8.93E-04	0.0012	8.14E-04
STD LSS Flex (rad)	2.15E-04	1.37E-04	1.45E-04	9.73E-05
RMS Gearbox Acc (rad/sec^2)	0.0168	0.0124	0.0155	0.0116
RMS Gearbox Jerk (rad/sec^3)	0.0226	0.0262	0.0212	0.0231
RMS Gearbox Speed Error (rad/sec)	0.0525	0.0319	0.0308	0.0188

Figure 5.3 – Normalized PI Controller vs Pole-Placement Statistics

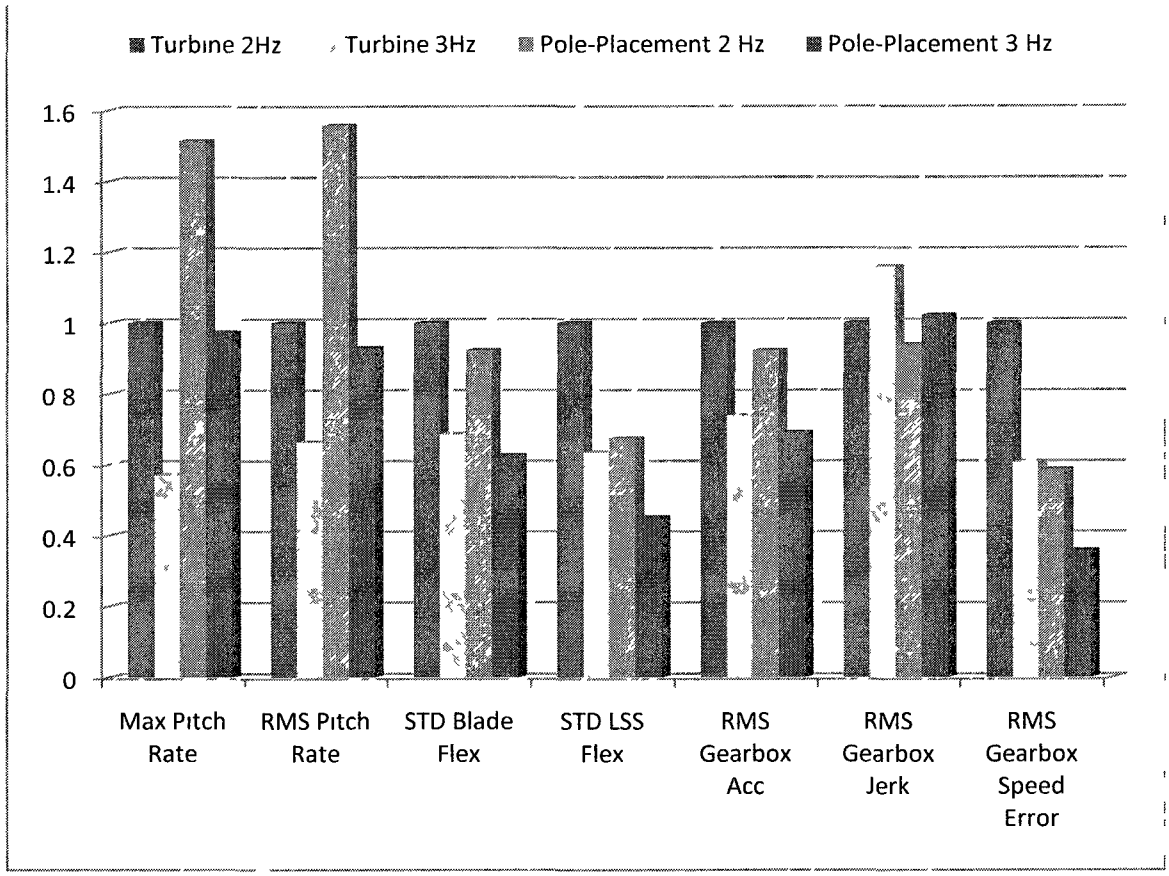

As can be seen from the chart above, and as noted previously, the Pole-Placement controller demands significantly more blade pitch command than the PI controller on the wind turbine only model. In the case of the pole locations chosen and implemented through full state feedback control, it can be seen that the blade pitch command is 150% higher than the turbine alone, and the RMS Blade Pitch command is also about 150% higher. Despite the much higher blade pitch commands required by

the controller, the other fatigue and component strain elements see a significant reduction.

Even with the higher pitch rates and command requirements it is interesting to note that the standard deviation of the Blade Flex for the pole-placement controller is about 12% lower. What this means is that although there is a higher strain being put on the blade pitch motor, by virtue of the larger pitch angles, the material fatigue of the blades is being reduced. The same can be said about the standard deviation of the low speed shaft. In this case the reduction is nearly 35%. As is the case with the blade flex the reduction in flex on the Low Speed Shaft can lead to longer lifespan just due to the reduction of the amount of twist within the shaft itself.

Some of the areas of greatest improvement with the implementation of this controller are seen on the gearbox itself. The error in the gearbox speed has been reduced by 50%. In addition the gearbox acceleration and jerks have both been reduced by 10%. This means that the earlier knowledge provided by the additional states within the model successfully allows the controller to shed excess energy sooner in the cycle. As a result, the turbine is capable of pitching the blades at the first indication of a wind speed change instead of waiting for the torque change due to wind speed to propagate itself through the system to be measured at the gearbox/generator shaft. The pole-placement controller can be further tuned to remove accelerations and jerks within the gearbox.

The design criterion for the pole-placement controller was to reduce the amount of generator speed variation. The thought behind this selection was that with less change in the gearbox speed, less torque variation would be transferred to the gear teeth. The results of Figure 5.3 show that there is the potential to further reduce the blade pitch commands to reduce the strain on the pitch motors while at the same time reducing generator speed error with respect to the turbine only model.

The multi-input LQR controller behaves much in the same way that the Pole-Placement Controller does. There are several distinct differences between the two controllers that actually allow the LQR controller to do a slightly better job of mitigating the torque variations in the wind turbine drive train. The biggest advantage of the LQR controller developed in this thesis is that it allows for two inputs instead of a single input. In effect this allows the plant to filter out higher frequency noise more effectively as the time constant of the fluid coupler is in the millisecond range, as previously noted in chapter 4. The other advantage that the LQR controller has over the pole-placement controller is a conceptual one. The LQR controller allows for state penalties to be chosen instead of assigning desired pole locations. The end result is that penalties can be manipulated and iterated in a controlled manner in order to minimize the effects of certain elements within the data model. The data comparison for the Multi-Input LQR Controller and the Turbine PI Controller is shown in Table 5.5 and Figure 5.4.

Table 5.5 – PI Controller Turbine Only vs Multi-Input LQR Controller with Fluid Coupler

	Turbine		LQR	
Parameter	2 Hz	3 Hz	2 Hz	3 Hz
Max Pitch Rate, (deg/sec)	0.4764	0.2725	1.5214	1.072
RMS Pitch Rate, (deg/sec)	0.2079	0.138	0.5165	0.3704
STD Blade Flex (rad)	0.0013	8.93E-04	0.001	7.40E-04
STD LSS Flex (rad)	2.15E-04	1.37E-04	1.07E-04	7.85E-05
RMS Gearbox Acc (rad/sec^2)	0.0168	0.0124	0.014	0.0111
RMS Gearbox Jerk (rad/sec^3)	0.0226	0.0262	0.0215	0.0239
RMS Gearbox Speed Error (rad/sec)	0.0525	0.0319	0.0197	0.0136

Figure 5.4 – Normalized PI Controller vs Multi-Input Statistics

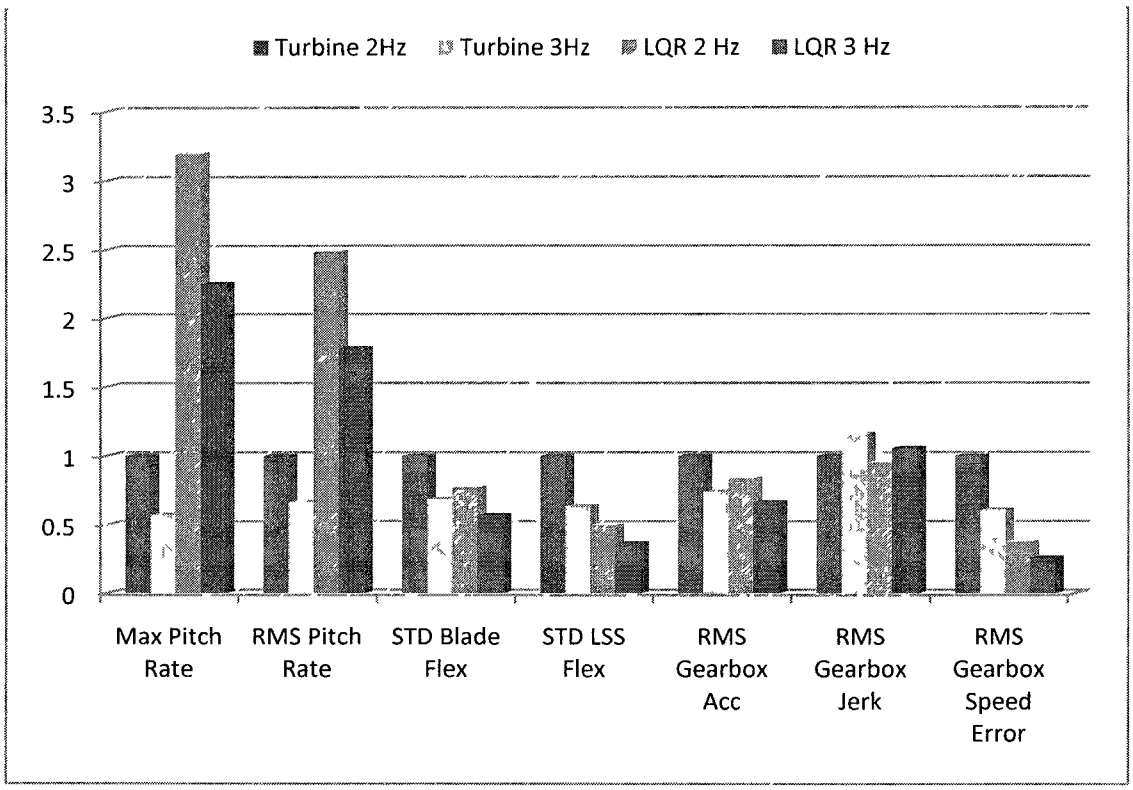

As previously seen with the Pole-Placement Controller, the LQR controller demands significantly more blade pitch command signal in terms of both the maximum pitch rate and the RMS pitch rate. In fact, the LQR controller is actually demanding nearly 310% more maximum blade pitch rate, and has an RMS blade pitch rate of 2.5 times that of the standard model wind turbine.

The tradeoff for the much higher blade pitch rates is that the stresses on the other components within the system are vastly improved. The speed regulation shows the greatest improvement with nearly a 78% reduction in the gearbox speed error. The other area of significant interest is the nearly 20% reduction in the accelerations seen on

the gearbox. The reduction in acceleration combined with the speed error indicates that there is the potential for significant improvement in the gearbox life span as the torque is related to rotational speed. Therefore, by reducing both the accelerations and the rotational speed variations, the torque variations seen within the gearbox and specifically on the gearbox teeth are reduced. The reduction of these torque variations may point to a longer lifespan of the gearbox in general, which is the main focus of this thesis.

The other two areas of the wind turbine that are also showing significant improvements are the values for the blade flex and the Low Speed Shaft flex. Both of these show nearly a 50% reduction in the overall stresses placed on the system. What is interesting to note in all of the different controllers is that although the desired purpose of the fluid coupler was to reduce the strain on the gearbox, it appears to have the added effect of reducing the strains on some of the other elements within the system, but not the blade pitch drives. In retrospect, this result should have been intuitive as the fluid coupler actually decouples both sides of the system from each other. What that means is that the fluid coupler actually provides a means of slippage to absorb sudden variations in the torque load caused by variations in the wind. In that respect both the rotor and LSS can unload energy without transferring the energy directly to the load. Instead the extra energy is dissipated in the form of heat in the coupler hydraulic oil which is then externally cooled.

Comparison of Fluid Coupler Controllers

Up until this point in the discussion of the simulation results, all of the controllers have been compared with the standard PI controller of a wind turbine that does not include a fluid coupler. Although this gives a relationship for how the controllers make improvements against the standard system, it does not provide a clear view of the improvements that more advanced controllers make within the same system. One of the major reasons for differences is that the controllers developed in this thesis are actually running much tighter control loops than the standard system. The result is that the blade pitch rates run higher and the speed regulation is tighter as shown in the previous analysis.

In order to compare the three controllers for the fluid coupler, I begin by looking at the data compiled from the 2 Hz wind file as that is the most severe in terms of the stresses that it places on the components and control system. The baseline for the comparisons will be the PI controller as was the case for the discussion above. As before, the results of the PI controller will be normalized to allow for visual comparisons of the data. As all of the data have been previously listed in Tables 5.3, 5.4 and 5.5, they will not be restated here. Instead only the normalized bar graph will be presented.

Figure 5.5 – Fluid Coupler Controller Comparisons

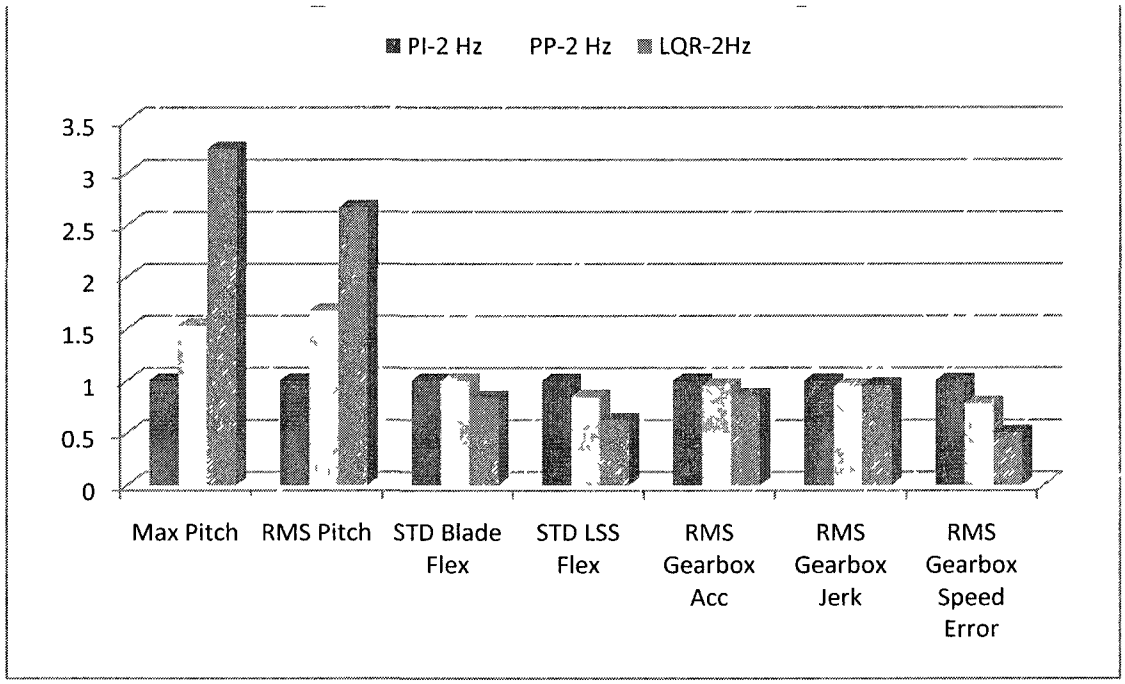

As noted previously the two advanced controllers do require more blade pitch control effort and as a result do have better fatigue and gearbox protection. In addition because of the added penalties that can be placed on the other states within the system, there is a significant improvement in the both the gearbox acceleration and gearbox speed error.

One of the items of concern in the data is the added strain is placed on the blade pitch motors. All three of the controllers developed have a significantly tighter control loop than the original wind turbine model. As a result, the system is demanding significantly more control effort to keep the gearbox speed error lower. This model is

simplified, and there are unmodeled dynamics that can potentially cause the control effort to exceed the rated values of the pitch control system. In addition to this limitation, it is not desired to trade the gearbox failure problem for pitch controller motor problems. In an effort to analyze this issue and make easy comparisons, the design criteria for the control system are modified slightly and the results are discussed below.

Design Criteria Change to Match Blade Pitch

As noted above, the controllers that were developed for this thesis were focused on the idea of minimizing the gearbox speed error, and by extension the generator speed error. The controllers developed here were shown to do a better job of regulating the speed of the generator by allowing the control loop to become tighter. As mentioned previously, the ability to develop the tighter control loop is a function of the fact that the fluid coupler within the drive train actually damps out one of the resonant frequencies of the standard turbine that is located right around 2 Hz. Because the fluid coupler damps out this resonant peak, the control loop can be run tighter without the fear of passing through an oscillatory frequency that would ultimately cause damage to the turbine or system.

In an effort to provide a comparison of what the fluid coupling system can do with similar blade pitch rates, two of the controllers, the PI Controller and the LQR Controller, had their control loops modified so that they would match the pitch rates of

the original system without the fluid coupler. The PI Controller and the LQR Controller were chosen specifically because they allowed for easy implementation of blade pitch rate penalties. As noted previously, the PI controller controls the blade pitch directly through the selection of the K_p and K_i gains. The LQR controller controls the blade pitch by placing an additional penalty in the R matrix. The pole-placement controller was eliminated from this part of the study because the placement of the poles does not allow for a direct correlation with the state that you are trying to change. As a result, the pole-placement controller requires significantly more iterations to garner the desired attribute changes.

To achieve similar blade pitch rates between the baseline wind turbine PI controller, the fluid coupler PI controller, and the LQR Controller, the following was done: the PI Controller gains $K_p$and K_i were left at to 3.60 and 0.350 respectively; the $r_{1,1}$ penalty in the LQR cost function was increased to 1500. As a result of these changes, the following results were found and are tabulated in Table 5.6 and shown in normalized form in Figure 5.6.

Table 5.6 – Standardized Blade Pitch Rate Statistics

Parameter	Turbine - 2 Hz	Fluid PI – 2 Hz	LQR - 2 Hz
Max Pitch Rate, (deg/sec)	0.4764	0.4711	0.5664
RMS Pitch Rate, (deg/sec)	0.2079	0.1937	0.3068
STD Blade Flex (rad)	0.0013	0.0012	0.0013
STD LSS Flex (rad)	2.15E-04	1.72E-04	1.87E-04
RMS Gearbox Acc (rad/sec^2)	0.0168	0.0163	0.0156
RMS Gearbox Jerk (rad/sec^3)	0.0226	0.0224	0.0208
RMS Gearbox Speed Error (rad/sec)	0.0525	0.0393	0.044

Figure 5.6 – Normalized Blade Pitch Controller Comparison

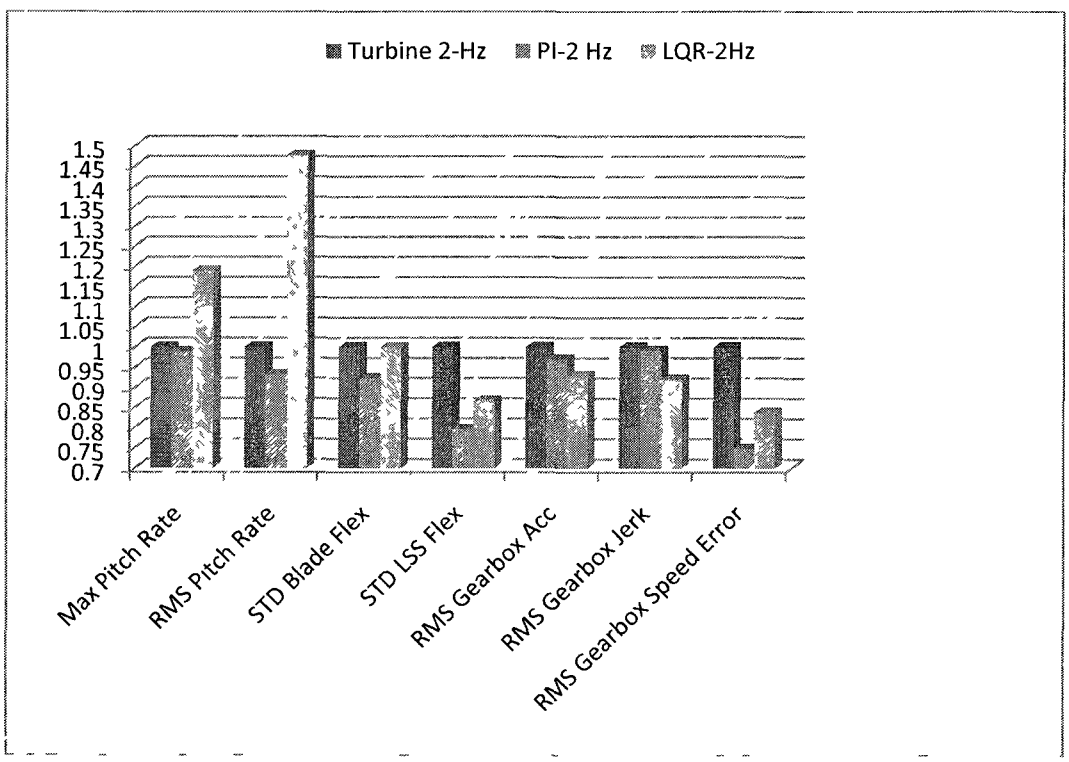

What can be ascertained from the data shown above is that even with the maximum blade pitch rates kept at nearly the same value, we see reductions in nearly all of the other parameters of interest. What is interesting to note from the above table is that even with the same pitch rates, the speed error when using the fluid coupler is lower in both the PI and LQR controllers than is the case when the coupler is not present. One of the other items that becomes evident by looking at the data is that the fluid coupler is acting to decouple the input side torque variations from the gearbox. This shows up in the reduction in the standard deviations of both the blade flex and the LSS flex. Because of the decoupling action of the fluid drive, neither the blades nor the low speed shaft are allowed to "load up" and then release all of their energy to the gearbox. That also shows in the fact that there is an approximately 5% and 10% reduction in the gearbox acceleration. This reduced gearbox acceleration translates into lower torque variation on the gearbox, which should lead to longer life spans for the gearbox itself.

CHAPTER 6:

CONCLUSIONS

Conclusions Based on Simulation Results

There are a number of original ideas included in this thesis, which include: the addition of a fluid coupler within the drive train, an original PI controller design for this model, designs for both a single input pole-placement controller and a multi-input LQR controller. Both of the advanced controllers make use of measurements from all the states of the wind turbine, and include the addition of a state that allows for zero steady state tracking error.

The primary theme throughout this thesis is the development of control systems to be used on a 5 MW wind turbine operating in region 3, the above rated power region. The model for the wind turbine is based on a previously derived linear model. However, the system presented in this thesis includes the addition of a theoretical model of a fluid coupler. The fluid coupler represents a significant change in the model from all previously derived control systems and techniques.

The goals of this study were to develop three different controllers: a PI controller, a single input Pole-Placement controller, and a multi-input LQR Controller, to control the behavior of the wind turbine in a narrow band of wind speeds around

18 m/s. The desired outcomes were to mitigate the torque variations that are allowed to reach the gearbox and to keep the blade angle changes to a level that was comparable or better than the already established levels for a wind turbine without the fluid coupler.

The properties of the fluid coupler were derived through iteration of the linear model. The fluid coupler itself is assumed to transmit power through a large damping element and a much smaller spring force element. The other elements, inertia and drag were able to be found in generalized literature about fluid couplers used in the marine industry. The values derived for the spring and damping elements of the fluid coupler were arrived at by forcing a known deviation in the output speed error of the gearbox. In this case the coupler was assumed to transmit 95% of the original input power to the gearbox, and it resulted in a speed reduction from approximately 1.22 rad/sec to 1.16 rad/sec.

The inclusion of the fluid coupler does allow for the addition of another control state, the coupling coefficient of the fluid coupler. This control is maintained by the position of a solenoid valve within the coupler itself. To maintain the simplicity of the models, this feature was only utilized in the multi-input LQR controller case. Both the PI controller and the pole-placement controller were assumed to have only one input, the blade pitch angle. By reviewing the results of this thesis, it can be seen that both of the advanced controllers, the pole-placement and LQR controllers, have the potential to provide better regulation of the torque variations that can propagate down the drive train. The pole-placement controller showed a 32% improvement in the RMS speed

regulation and 9% gearbox jerk reduction as compared with the wind turbine model with fluid coupler utilizing a PI controller. The better regulation comes at the expense of allowing the blades a larger maximum pitch rate. This is despite the fact that the pole-placement controller includes feedback from additional states that allow the blades to begin pitching earlier based on the torque variation being available sooner. The added pitch rate variation allows a much tighter control loop. This is made possible by the shift in the Bode response that eliminates the resonant hump at 2 Hz in the original turbine model that did not include the fluid coupler.

The multi-input LQR controller showed even greater increases in the blade pitch angle rate and a 66% improvement in the speed regulation and 9% reduction in the gearbox jerk. Because of the addition of the state due to the fluid coupler, the RMS errors and gearbox accelerations were significantly lower than were seen on either the pole-placement or PI controller models. The control that was previously applied to the blades was instead allowed to be taken up in both the blades and the solenoid valve. Additionally, because the solenoid value was able to react to changes much quicker than the blades it was better able to damp out the higher frequency changes in the wind and allowed the controller to better regulate the speed of the gearbox.

The item that is of greatest importance to this model is the addition of a fluid coupler into the system. The inclusion of the coupler in the model results in a significant change in the Bode plot for the open loop wind turbine system. The wind turbine system without the fluid coupler has been shown in previous research to have a resonant peak at approximately 2 Hz (9). However, as shown in chapter 2, the addition

of the fluid coupler removes this peak and actually provides a significant amount of attenuation for all frequencies above 1 Hz. What this means is that the power in these higher harmonics are actually filtered in the plant and are not reaching the gearbox. It further shows that the delay in between the wind speed change and the blade pitch command does not cause as dramatic an increase in the torque reaching the gearbox.

The addition of the large damping element (the fluid coupler) within the model has an additional benefit, i.e. the overall plant is easier to control. It also makes the controller more robust, and it can allow for larger tolerances in the parameter estimates and modeling inaccuracies. Because this model is easier to control, larger control efforts can be placed on the blade pitch angles to mitigate the low frequency torque variations. The higher frequency variations are allowed to damp out within the fluid coupler rather than propagating down the drive shaft and reaching the gearbox. The results of the simulation also show that by keeping the maximum pitch angle rates the same for the original model without the coupler and the model with the coupler, a standard PI controller can provide a 23% reduction in generator speed error. This is significant in that the better regulation indicates that there are fewer large torque variations that reach the gearbox.

The fluid coupler itself provides an additional mechanical advantage that cannot be clearly shown in the model. Because the fluid coupler does not have a rigid connection between the input rotor shaft and the gearbox drive shaft, it can allow the two elements to be spinning at slightly different velocities. This means that the blades and rotors are actually somewhat decoupled from the gearbox and generator. Because

the systems are decoupled, changes in torque as seen by the blades and rotors are not necessarily transferred thru the fluid coupler and into the gearbox and generator through conservation of energy principles.

The more advanced controllers mitigate torque variations better than a PI controller. However, this study concludes that the additional state feedback and estimation needed for pole-placement or LQR control do not provide enough improvement in the system responses to warrant their use in this system. Among the different controllers there was less than an 8% improvement in the RMS jerk on the gearbox, and a 5% reduction in the gearbox acceleration when the blade pitch rates were kept to approximately the same level. Significant improvement is observed in the overall loading and fatigue on the blades and low speed shaft. The addition of the fluid coupler removes the direct coupling link between the spinning blades/rotor and the gearbox. It is this decoupling factor that leads to the conclusion that it is the addition of the fluid coupler that is most significant in reducing the torque variations on the gearbox, and not necessarily the additional feedback states of the advanced controllers. Furthermore, the robust nature of the system provides the system with significant stability margins such that the added margins that can be gained from the full state feedback controllers are not required.

In addition, one must also act for the added complexity of the more advanced control techniques. In the case of the pole-placement and multi-output LQR controllers, it is required that all of the states are either measured directly or estimated through an observer. In the case of added sensors this can lead to longer term maintenance issues

for the wind turbine. Now, instead of having a preventative maintenance (PM) schedule for just the encoder on the generator shaft, there must be also be PM schedules for all of the additional sensors needed to provide the values for all of the other states within the turbine. This can potentially lead to additional down time for the turbine.

The added sensors have one further disadvantage. The addition of all the extra control loops makes the system harder to trouble shoot when a failure occurs. Any failures would require the technician to trace any number of sensor wires to find the system error instead of the single input needed for the PI Controller. In the case where the system states are estimated from an observer or Kalman filter, the controller must become digital to enable the computer routines to predict the values of all the states. This would require more upfront modeling work to ensure that all the parameters of the model are correct. As mentioned earlier, even though this is possible, the advantages to making this switch are outweighed by the simplicity and robustness of a standard PI controller.

Suggestions for Future Study

This study has focused on the hypothetical addition of a fluid coupler to provide a proof of concept. While fluid couplers of the size and scope needed to implement the damping on systems of this size do exist for the marine industry, they have not yet been implemented in wind turbines of this size. There are a number of studies that will need to be done with regard to the added weight factor by adding these items within the nacelle. The added weight of the fluid coupler itself is not deemed to be insignificant.

Because of that, there are going to be a number of added loads and fatiguing issues with the towers that have not been included in this study.

In addition to these uncertainties, all of the equations developed for the fluid coupler have been idealized to show that something like this could work. Both the damping coefficient and the spring constant for the fluid coupler are based on assumptions of how the fluid coupler would behave in the system. As a result, the values used throughout this thesis were hypothesized. Further study should be taken up in the actual modeling of the fluid coupler. This would include modeling the non-linearities within the fluid coupler. It would also include a study of how the coupler would behave in regions 2 and 2 1/2 so that there is still a smooth transition between regions and that the fluid coupler does not drastically increase the cut-in wind speed need to begin the wind turbine operation.

The selection of a hydraulic coupling fluid is another area that needs to be investigated. This study assumed a constant state fluid. It did not take into account any changes in fluid properties over time based on temperature, fluid cleanliness, or degradation of the fluid due to aging. It also does not take into account any changes in the fluid properties due to pressure variations.

This study focused on only one range of operating points for the wind turbine operation. Further work needs to be done using the linearized equations throughout the entire operating range of region 3. This would include investigations into the shut-down region of the machine. Based on the initial results of this study, it would suggest that the addition of the fluid coupler would allow for an increase to this transition point.

The models used in this thesis are low order, simplified models. One example of this is modeling all of the blades as a single element. For the higher complexity controllers, the Pole-placement and LQR controllers, to operate properly on the real system, the system models must be much more detailed. This is because each of these types of controllers apply feedback gains from all of the states within the model/plant. That would mean that each of the blades should have its own model and each of their respective torques would be additive in the model.

Another area for further research would be using the individual blade flex dynamics to control the system instead of the generator speed. A change to this type of system potentially allows for a number of advantages when combined with a fluid coupler to help damp out torque variations. The first advantage is that by measuring the blade flex, the system has the earliest possible indication of a wind speed change. That means that any controller can react more quickly to any torque changes as they do not have to pass through the entire system before being detected. If the blades can be pitched independently of each other then there is even greater advantage that can be gained. By setting three precise measurement positions on the blades, one can actually produce lead information for the next blade coming around. In that way, the individual blades can be pre-pitched to further smooth out variations in wind speed within the entire blade field and keep a constant torque. When this type of individual blade control is combined with the fluid coupler there should be significant reductions in the jerk seen in the gearbox.

One additional item that would need to be studied if individual blade control was implemented is the lifetime/wear cycle on the blade pitch motors. The overall objective needs to be the reduction in down time of the wind turbine, and trading one problem for another does not advance the technology. In addition to the wear and tear on the pitch motors, there will likely be additional strain on the towers and all of the bearings. This is due to the potential of having the blades at three different angles and as such there can potentially be a change in the rotational center of gravity of the blades.

LIST OF REFERENCES

1. **Wikipedia.** History of Wind Power. *Wikipedia.* [Online] June 2011, 9. [Cited: June 20, 2011.] http://en.wikipedia.org/wiki/History_of_wind_power.

2. **Dodge, Darrell M.** Wind Power - An Illustrated History of its Development. *Wind Power Development Index.* [Online] TelosNet Web Development, 2006. [Cited: January 11, 2011.] http://www.telosnet.com/wind/index.html.

3. *A Brief History of Wind Turbine Industries in Denmark and the United States.* **Jens, Vestergaard, Lotte, Brandstrup and Goddard, III, Robert D.** s.l. : Academy of International Business (Southeast USA Chapter) Conference Proceedings, November 2004.

4. **World Wind Energy Association.** World Wind Energy Association-Home Page. *World Wind Energy.* [Online] WWEA, 2006. [Cited: November 30, 2010.] http://www.wwindea.org/home.

5. **Northern Power.** The Gear-Box Problem. *Northern Power Sytems.* [Online] July 2009. [Cited: December 14, 2010.] http://www.northernpower.com/pdf/the-gearbox-problem.pdf.

6. **Clemson University.** Clemson University News Room. *Next Generation Wind Turbines.* [Online] November 23, 2009. [Cited: June 20, 2011.] http://www.clemson.edu/media-relations/article.php?article_id=2432.

7. **United States Department of Energy.** *20% Wind Energy by 2030:Increasing Wind Energy's Contribution to U.S. Electricity Supply.* s.l. : United States Department of Energy, 2008. DOE/GO-102008-2567.

8. **Renewable Energy UK.** Calculation of Wind Power. *REUK Calculation of Wind Power.* [Online] April 18, 2008. [Cited: June 20, 2011.] http://www.reuk.co.uk/Calculation-of-Wind-Power.htm.

9. **Aho, Jacob.** *Advanced Control of Large Scale Wind Turbines.* MS Thesis ECE Department : University of New Hampshire, 2010.

10. **Wright, Allan D and Fingersh, L. J.** *Advanced Control Design for Wind Turbines-Part I: Control Design, Implemenation and Initial Tests.* Golden, CO : National Renewable Energy Laboratory, 2008. Technical Report.

11. **Jonkman, J., et al.** *Definition of a 5-MW Wind Turbine for Offshore System Development.* Golden, CO : National Renewable Energy Laboratory, 2009. Technical Report.

12. **Peerless Pump.** Peerless Pump Hydroconstant Variable Speed Fluid Drives: Technical Bulletin. *Peerless Pump.* [Online] July 2006. [Cited: January 28, 2011.] http://www.northernpower.com/pdf/the-gearbox-problem.pdf.

13. **Voith Turbo GmbH & Co. KG.** Hydrodynamics in Drive Technology. *Voith Turbo: Fluid Couplings Literature.* [Online] Voith Turbo, February 11, 2009. [Cited: March 11, 2011.] http://www.voithturbo.com/sys/php/docdb_stream.php?pk=2848.

14. **Pressman, Abraham I.** *Switching Power Supply Design, Second Edition.* New York, New York : McGraw-Hill, 1998.

15. **Nise, Norman S.** *Control Systems Engineering, Fifth Edition.* Hoboken, New Jersey : John Wiley & Sons, 2008.

16. **Brogan, William L.** *Modern Control Theory.* Upper Saddle River, NJ : Prentice-Hall, 1991.

17. **Lewis, Frank L. and Syrmos, Vassilis L.** *Optimal Control, Second Edition.* New York, NY : John Wiley and Sons Inc, 1995.

18. **Slotine, Jean-Jaques E. and Li, Weiping.** *Applied Nonlinear Control.* Upper Saddle River, New Jersey : Prentice Hall, 1991.

19. **White, Frank M.** *Fluid Mechanics, Fifth Edition.* New York, New York : McGraw-Hill, 2003.

20. **Cape Wind Energy.** Cape Wind Energy: Index. *Cape Wind.* [Online] eCape, Inc, 2010. [Cited: January 7, 2011.] http://www.capewind.org/index.php.

21. **Ogata, Katsuhiko.** *Modern Control Engineering.* Englewood Cliffs, NJ : Prentice-Hall, 1970.

22. **Pease, Dudley A.** *Basic Fluid Power.* Englewood Cliffs, NJ : Prentice-Hall, 1967.

23. **D'Azzo, John J. and Houpis, Constantine H.** *Linear Control System Analysis and Design.* New York, NY : McGraw-Hill, 1995.

24. **Kuo, Benjamin C.** *Automatic Control Systems.* Englewood Cliffs, NJ : Prentice-Hall, 1995.

25. **Norvelle, F. D.** *Electohydraulic Control Systems.* Upper Saddle River, NJ : Prentice-Hall, 2000.

26. **Brown, Robert Grover and Hwang, Patrick Y.C.** *Introduction to Random Signals and Applied Kalman Filtering.* New York, NY : John Wiley and Sons, 1997.

APPENDIX A:

MATLAB SCRIPT FILE POLE-PLACEMENT

```
% Wind Turbine 5MW Model Parameters June 2011%
% Blade Inertia distributed so that most inertia is included in rotor, not in
% flexible blade section model%
clear all
clc
format compact
Po=5E6
Wgo=12.1*pi/30 %Gearbox speed%
No=1/97
wn=1.07*2*pi
N = 97
N2 = N*N
Jb = 3*1.176E7
tauB=0.2;
dt_db = 0.24823;
dt_dw = 0.3258;

Jr = 1.15E5;
Br = 11000;
Dr = 6.22e6;
Kr = 867.6e6;

%Set Model for a 5 percent fluid slip

Jf = 33e3*0.4; %fluid Inertia
Df = 62.2e6*1.2; %Damping Coefficient
Kf = 8e6/10000; %Fluid Spring Coefficient
Bf = .2*Jf;
Jg = 5.34E2;
Bg = 6;

JL = .04
BL = Po/(Wgo/No)^2
```

```
JG = N2*(Jg + JL)
BG = N2*(Bg + BL)

%Shift part of blade inertia to rotor%
Jr=Jr+Jb/2;
Jb=Jb/2;
Db=8*Jb;
Kb=16*Jb;
Bb=0;

roots([Jr Dr Kr])
roots([Jb Db Kb])
roots([JG BG])

A=[0 -1 0 0 0 0 0 0;
   0 -(BG+Df)/JG Kf/JG Df/JG 0 0 0 0 ;
   0 -1 0 1  0 0 0 0;
   0 (Df/Jf) -(Kf/Jf) -(Dr+Df+Bf)/Jf Kr/Jf Dr/Jf 0 0 ;
   0 0 0 -1 0 1 0 0 ;
   0 0 0 (Dr/Jr) -(Kr/Jr) (-Br-Dr-Db)/Jr Kb/Jr Db/Jr;
   0 0 0 0 0 -1 0 1;
   0 0 0 0 0 Db/Jb -(Kb/Jb) -(Bb+Db)/Jb;]
R=eig(A)
   B=[0;0;0;0;0;0;0;Jb/4.76];
   C=eye(8);

P=[ -1.0935*1e+007
    -8.0+10.0i
    -8.0-10.0i
   -6129.5
    -18
  -.2000
 -0.0000107
 -2.0548];
K=place(A,B,P)% set the desired pole locations
X= transpose(eig (A-B*K));% check closed-loop eigen values
Ca=[0 1 0 0 0 0 0 0];
D=[0;0;0;0;0;0;0;0];
X(1,1)%List individual closed loop-pole Locations
```

X(1,2)
T=[X(1,3),X(1,4),X(1,5),X(1,6),X(1,7),X(1,8)]

APPENDIX B:

MATLAB SCRIPT FILE MULTI-INPUT LQR

```
% Wind Turbine 5MW Model Parameters LQR June 2011%
% Blade Inertia distributed so that most inertia is included in rotor, not in
% flexible blade section model%
clc
format compact
Po=5E6;
Wgo=12.1*pi/30; %Gearbox speed%
No=1/97;
wn=1.07*2*pi;
N = 97;
N2 = N*N;
Jb = 3*1.176E7;
tauB=0.2;

Jr = 1.15E5;
Br = 11000;
Dr = 6.22e6;
Kr = 867.6e6;
dt_db = 0.24823;
dt_dw = 0.3258;

%Set Model for a 5 percent fluid slip

Jf = 33e3*0.4;
Df = 62.2e6*1.2;
Kf = 8e6/10000;
Bf = .2*Jf;
Jg = 5.34E2;
Bg = 6;

JL = .04;
BL = Po/(Wgo/No)^2;
```

```
JG = N2*(Jg + JL)
BG = N2*(Bg + BL)

%Shift part of blade inertia to rotor%
Jr=Jr+Jb/2;
Jb=Jb/2;
Db=8*Jb;
Kb=16*Jb;
Bb=0;

roots([Jr Dr Kr])
roots([Jb Db Kb])
roots([JG BG])


A=[0 -1 0 0 0 0 0 0;
   0 -(BG+Df)/JG Kf/JG Df/JG 0 0 0 0 ;
   0 -1 0 1  0 0 0 0;
   0 (Df/Jf) -(Kf/Jf) -(Dr+Df+Bf)/Jf Kr/Jf Dr/Jf 0 0 ;
   0 0 0 -1 0 1 0 0 ;
   0 0 0 (Dr/Jr) -(Kr/Jr) (-Br-Dr-Db)/Jr Kb/Jr Db/Jr;
   0 0 0 0 0 -1 0 1;
   0 0 0 0 0 Db/Jb -(Kb/Jb) -(Bb+Db)/Jb;]
R=eig(A)
   B=[0 0;0 0;0 0;0 1/Jf;0 0;0 0;0 0;Jb/4.76 0];

Ca=[0 1 0 0 0 0 0 0];
D=[0;0;0;0;0;0;0;0];

q=eye(8)- eye(8); %Create a Zero Q-Matrix (8x8)
r=[15,0;
   0,.0000025];
q(1,1)=150;
q(2,2)=100;
q(3,3)=1000;
q(4,4)=900;
q(5,5)=1000;
q(6,6)=5000;
q(7,7)=800;
q(8,8)=500;
```

```
q;
[K,S,E]=lqr(A,B,q,r);
%X= transpose(eig (A-B*K));
E(1,1)%List Pole Locations
E(2,1)
T=[E(3,1),
E(4,1),
E(5,1),
E(6,1),
E(7,1),
E(8,1)]
T(5,1)%Show Location of Slow Pole
K
```

APPENDIX C:

MATLAB SCRIPT FILE RMS

```
function RMS (a)
sqrt(a'*a/size(a,1))
end
```

APPENDIX D:

SIMULINK® MODELS

PI-Controller

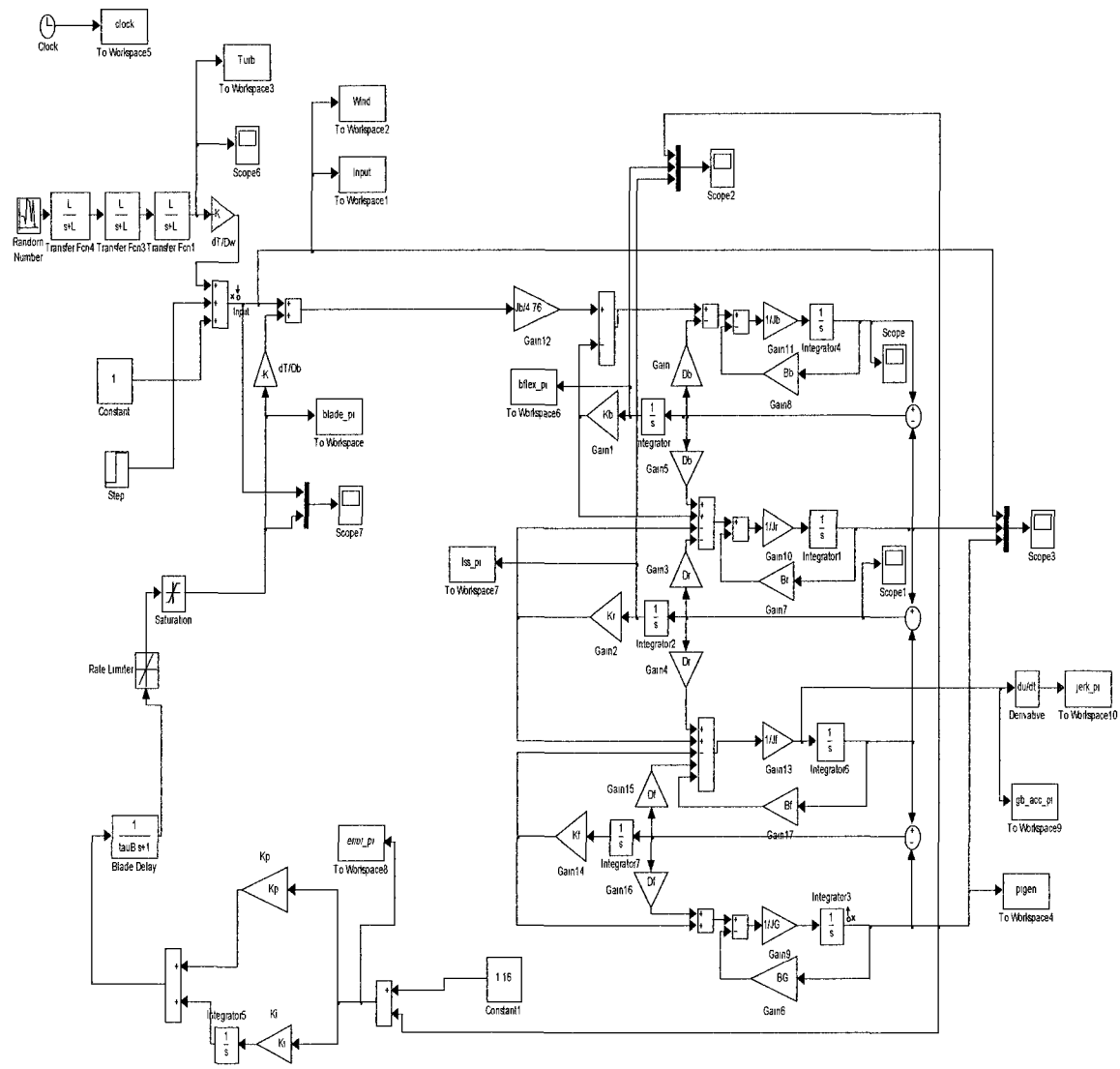

Pole-Placement

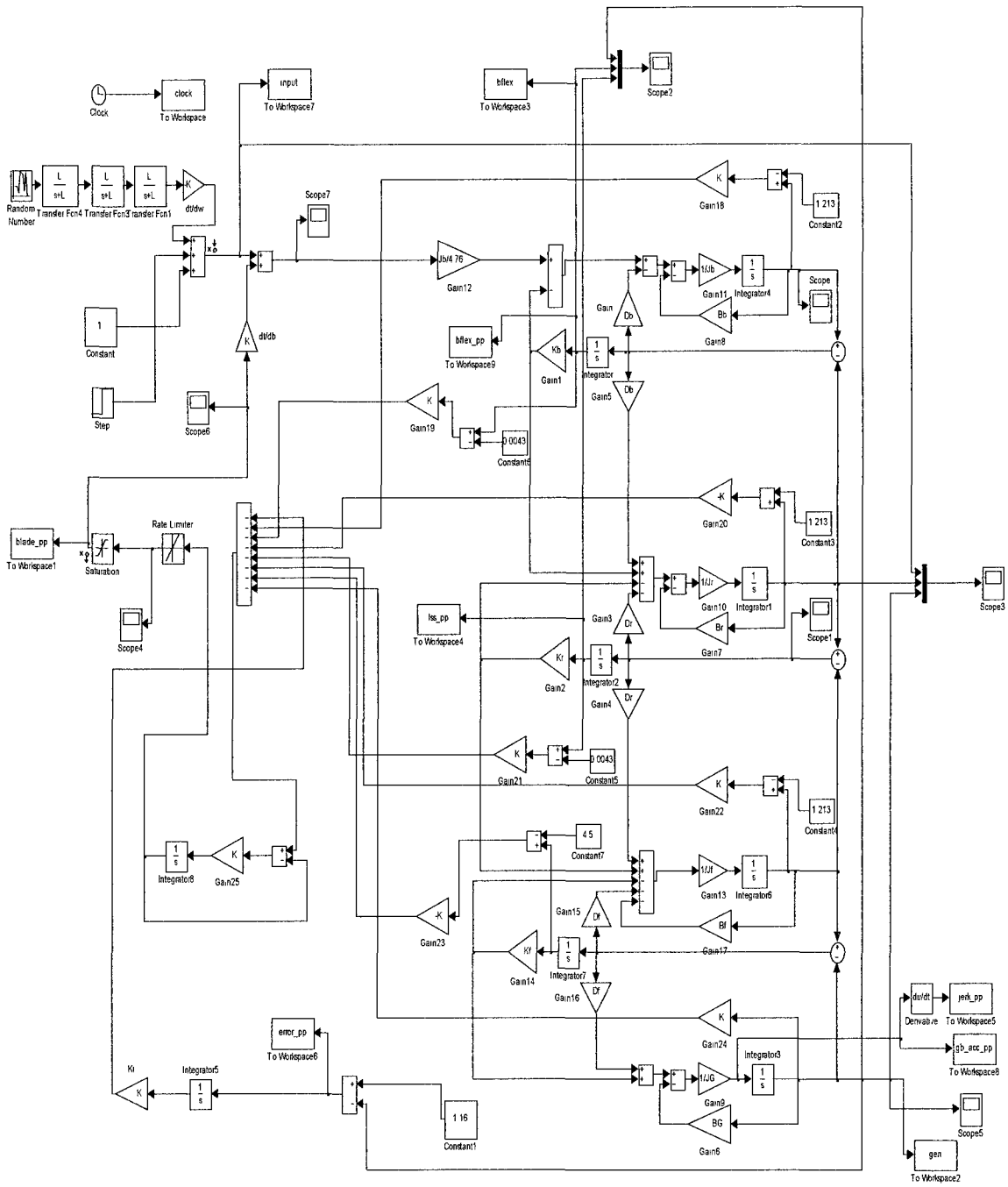

Multi-input LQR